The Bauschinger Effect In High Strength Steels

Thesis

UNRESTRICTED

THE BAUSCHINGER EFFECT IN HIGH STRENGTH STEELS

Peter Brown, B.Eng(Hons)

M. Phil.

The Open University

Materials Discipline

1995

Date of submission: 25 May 1995
Date of award: 16 November 1995

ABSTRACT

The aim of this investigation was to characterise the Bauschinger effect (BE) exhibited by Q2N, a high strength, martensitic steel. It is defined here as *"the phenomenon by which the flow stress of a metal in one direction, is reduced by plastic flow in another"* and the uniaxial tension/compression test is adopted as the most appropriate mechanical test for studying the BE in Q2N. The BE is assessed by a series of primary parameters which characterise it in terms of a specific quantity, and by a range of secondary parameters which express the BE as a fraction of its theoretical maximum. The effects of tensile prestrain and heat treatment on both groups of stress, strain and energy related BE parameters is addressed and a theoretical analysis based on the Parallel Elements Model (PEM) and the Atkinson, Brown, Stobbs (ABS) model of the BE is also considered.

The results show that all of the primary BE parameters, and the stress related secondary BE parameter increased linearly with prestrain, indicating that the BE in Q2N also increased with prestrain. However, the strain and energy related secondary BE parameters decreased exponentially with prestrain, demonstrating a decrease in the BE exhibited by Q2N with prestrain. Whilst no attempt is made to resolve this dichotomy it is emphasised that the BE in Q2N can only be fully characterised, if it is quantified using **all** of the stress, strain and energy related BE parameters, both primary and secondary.

It is also demonstrated that a low temperature, short duration heat treatment can reduce the BE in Q2N by 25%, and that for prestrains below 1% agreement between experimental data and the predictions of the PEM/ABS model of the BE is good.

It is concluded that Q2N exhibits a substantial BE which may adversely affect the performance of any structure fabricated from it.

DECLARATION

This is to certify that, except where specific reference to others is made, the work described in this thesis is the result of the candidate's own investigation, and has not previously been submitted to The Open University, or any other university/institution, for an award of any kind.

Candidate

ACKNOWLEDGEMENTS

Whilst the title page of this thesis bears the name of only one author, it would be both unkind and unethical if I failed to acknowledge in full, the guidance and encouragement I have received from my friends and colleagues during the course of this work.

My gratitude must go first and foremost to Karen, my wife, who has spent many weekends on her own caring for our two young children, Katherine and James. Without her support and hard work, it would not have been possible to even begin this work, let alone complete it, and I would like her to know that I love her very much, and that I greatly appreciate the personal sacrifices she has made to enable the advance of my career.

I would also like to acknowledge the advice and counsel of my external supervisor, Professor Bill Plumbridge, Head of the Materials Discipline at The Open University, whose help far exceeded the bounds of his obligation.

Finally, I would like to thank Dr David Creswell and my internal supervisors, Mr Greg Mitchell and Mr John Bird, of the Defence Research Agency, not only for funding this research, but for providing me with an opportunity to better myself, when others felt unable to do so.

CONTENTS

CHAPTER 1

THE BAUSCHINGER EFFECT IN HIGH STRENGTH STEELS

1.1 Introduction

The Bauschinger effect, first reported in 1881 [1], and later published in English in 1886, was described as follows:-

'.... an annealed rod of steel, which had been overstrained in tension, exhibited increased resistance to a tensile stress, but reduced resistance to compression ....'

Since then, it has been studied in a wide range of materials by numerous workers, aiming to discover more about both its origin and magnitude.

There are a variety of definitions for the Bauschinger effect [2,3-7], but that provided by MacEwen *et al* [8], has the advantage of being short, and to the point:-

'The Bauschinger effect describes the phenomenon by which, the flow stress of a metal in one direction, is reduced by plastic flow in another.'

The term 'flow stress' should **not** be misinterpreted as meaning a yield stress. Instead, it simply refers to the stress developed after a certain amount of plastic strain, in a direction which is not coincident with the direction of forward prestraining, and is more akin to a proof stress.

For example, Lay *et al* [9] have reported that the high strength steel Q2N, in its fully quenched and tempered condition, has a 0.2% compressive proof stress , $0.2\%\sigma_R$, of 820 MPa. After a tensile prestrain of 2%, this was reduced by more than 45% to 448 MPa, demonstrating that the Bauschinger effect (BE) can have a significant impact on the mechanical properties of this steel.

Q2N is currently being investigated by the Defence Research Agency (DRA), as a possible primary pressure hull material to be used in the construction of submarines for the Royal Navy. The chemical composition of Q2N, Table 1, stipulated in Naval Engineering Standard 826 [10], shows it to be a low carbon steel, with chromium, nickel, molybdenum and vanadium as its principal alloying elements, which has a carbon equivalent of approximately 0.70%.

The microstructure of Q2N in its fully quenched and tempered condition consists of tempered martensite with a grain size of approximately 10μm, Figure 1a, containing a fine dispersion of spherical carbides, Figure 1b. This alloy exhibits a 0.2% tensile proof stress , $0.2\%\sigma_F$, of between 690 - 790 MPa, a minimum elongation of 20%, a reduction of area of at least 50%, and a $0.2\%\sigma_F$ to ultimate tensile strength ratio which should not exceed 0.88. In addition, Q2N is also required to exhibit a Charpy impact energy of not less than 80 joules at -84°C, Figure 2 [11]. Whilst the tensile properties of Q2N have been fully characterised, [12] research into its compressive properties, and the BE it exhibits; where the compressive strength of Q2N is reduced as a result of being previously loaded in tension, and visa versa; has been limited [9]. However, there is growing interest in obtaining an improved understanding of the mechanism of submarine collapse at maximum diving depth. Although there is very good agreement between recent theoretical strength predictions and actual collapse pressures recorded experimentally during the testing of large scale submarine models, such calculations have so far been based on relatively simplistic assumptions regarding the shape of the pressure hull material stress/strain curve, with no allowance being made for the influence of the BE, [13].

For example, consider a submarine pressure hull constructed from a number of 50mm thick plates of Q2N, which have been rolled to a radius of 5m from flat stock, Figure 3a. At maximum diving depth, collapse of the pressure hull may occur by the development of six plastic hinges, whereby localised regions of the pressure hull are forced out of circularity by the external water pressure,

Figure 3b. For this particular collapse mode, the internal surfaces of hinges A, B & C, which were subjected to a compressive load whilst being rolled to the required radius, are now in tension. Their corresponding external surfaces however, which experienced a tensile load during rolling are now in compression. Consequently, because of this reversal in loading conditions which may occur during collapse, any analysis of the strength of these hinges will need to incorporate the influence of the BE on their reverse yield strength. Recent work [13] has indicated that the BE may reduce submarine maximum dive depths by as much as 20%. Consequently, one of the principal aims of this report will be to investigate the origin of this effect and its magnitude in Q2N.

The remainder of this report examines various definitions of the BE, discusses testing techniques and parameters which have been used to quantify it, and highlights those most appropriate to Q2N. Attention is then focused on the BE in pure metals and single phase alloys in order to pin point a number of microstructural features which affect its magnitude, and give some indication as to its origin. The BE in two phase and dispersion hardened alloys, such as Q2N, is also considered, as these materials can be modelled as a plastically deformable matrix containing a fine dispersion of hard second phase particles. An analysis of this model by Atkinson *et al* [2]and its relevance to Q2N is discussed.

CHAPTER 2

LITERATURE REVIEW

2.1 Tests used to measure the Bauschinger effect

The most commonly adopted procedure for determining the extent of the Bauschinger effect is the uniaxial tension/compression test, with the uniaxial compression/tension test also being popular. The uniaxial tension/compression test (TC), involves plastically deforming a specimen in tension to a predefined strain; usually referred to as the *prestrain*; at which point the direction of deformation is reversed, and testing is completed by plastically deforming the specimen in compression.The extent of reverse plastic strain experienced by the specimen during such a test, is frequently restricted by the difficulty of maintaining axiality over an extended strain range, before buckling occurs. For this reason, the amount of compressive engineering strain that can usually be achieved is often no greater than approximately 10% [14]. The uniaxial compression/tension test (CT) is identical to the TC test, with the exception that the specimen is prestrained in compression, unloaded and then tested in tension. The initial direction of prestrain appears to have little influence on the magnitude of the Bauschinger effect, [15]. However, in cold drawn patented steel wire [16], and an aluminium composite containing whiskers of SiC [17], it has been found that the BE is greater if the direction of prestrain is compressive. This was attributed to the presence of residual stresses introduced in to test material by processes such as deep drawing prior to the manufacture of test pieces. As Q2N steel plate is given a full quench and temper heat treatment after being rolled to thickness, assymetry in the BE as a function of the direction of prestrain is unlikely to be observed.

Another less widely used Bauschinger test is the reversible torsion test (RT) [6-7, 18-19]. A thin cylinder or rod is plastically deformed in one direction by the application of a torque which is achieved by twisting it through an angle ϕ_F, the magnitude of which is dependant upon the level

of shear prestress (τ_F) or shear prestrain (γ_F) to be applied. The direction of deformation is then reversed by twisting the specimen through a reverse angle of ϕ_R,and testing is usually considered to be complete when the magnitude of the reverse shear stress ,τ_R, equals τ_F. One advantage of the RT test is the ease with which considerable amounts of plastic deformation can be achieved, which is particularly useful in studying the effect of large prestrains on the BE in ductile materials. Woolley [7] for example has characterised the BE in copper and aluminum using torsional shear prestrains in excess of 100%.

The TC, CT and RT tests have principally been employed in determining the magnitude of the BE in bulk material. In the case of thin sheet material however, one approach has been to adopt the planar simple shear or PSS test [20], Figure 4. The shear stress/strain curve obtained from a PSS test, is similar to that of a TC, CT or RT test, and although the Bauschinger parameters (discussed later) derived from such a test are not identical to those previously mentioned, they are closely related and have provided useful information about the Bauschinger effect in rimmed and semi-killed sheet steels.

The BE may also be measured by X-ray diffraction techniques in determining the internal stresses within a specimen during forward and reverse straining. Wilson & Konnan [21], demonstrated by means of X-ray line broadening techniques, that when a high carbon steel with a microstructure containing a fine dispersion of cementite particles in a ferrite matrix, was given a tensile prestrain of 3%, the internal stress system which developed upon unloading was directional. Tensile stresses within the cementite particles were balanced by compressive stresses, $<\sigma>_M$, in the surrounding ferrite matrix. Because the ferrite matrix was already in compression after unloading, reverse straining resulted in premature compressive yielding, and the Bauschinger effect was observed. Such experiments and the analysis of the results is both theoretically and technically demanding, and they have not been repeated by other workers. However the findings have been

extremely useful in that they pinpoint a possible mechanism for the origin of the Bauschinger effect, particularly in the case of materials containing a fine dispersion of hard second phase particles, such as Q2N.

Vickers hardness measurements [22] have also been used to determine the residual back stress in the matrix of materials containing a fine dispersion of hard second phase particles after prestraining. It is not possible to calculate absolute values of $<\sigma>_M$ from such data but the effects of forward and reverse straining on $<\sigma>_M$ can at least be monitored to some extent by changes in hardness levels. Another more quantitative approach has been to measure the dimensions of prestrained specimens before and after being stress relieved [22]. The strains generated during stress relief were assumed to be a result of the complete relaxation of any residual back stresses present within the prestrained specimens. Values of $<\sigma>_M$ calculated from these strain measurements were found to be lower than those determined by X-ray broadening techniques and were assumed to represent the lower bound in obtaining accurate measurements of matrix back stresses.

A novel attempt at investigating the Bauschinger effect has been to measure the acoustic emissions of specimens during forward and reverse straining [23]. As yet the results are inconclusive.

2.2 Parameters used to quantify the Bauschinger effect

A typical T/C test stress/strain curve for Q2N is presented in Figure 5a. Such data can also be represented in terms of 'absolute' stress and cumulative strain, in which the compressive cycle of the TC test is re-plotted in the $+\sigma/+\epsilon$ quadrant of the σ/ϵ diagram, for ease of comparison with the initial tensile cycle, as shown in Figure 5b. These figures illustrate a number of distinctive features which may be used to characterise the BE exhibited by Q2N :-

1. The absolute value of the reverse 0.2% compressive proof stress , $0.2\%\sigma_R$, is less than the forward tensile flow stress at the point of stress reversal, σ_F, Figure 6a.
2. The reverse compressive flow stress curve exhibits a much higher degree of work hardening than the forward tensile flow stress curve. However, this high of work hardening can be reduced by heat treatment after prestraining, and is therefore termed *transient* softening, Figure 6a.
3. After the first few percent deformation, the reverse curve essentially becomes parallel with the forward curve, but at equivalent strains the absolute value of the reverse flow stress, is less than that of the forward flow stress. This difference is referred to as *permanent* softening and is denoted by $\Delta\sigma_P$, Figure 6b.

Each of the above characteristics can be combined in various ways to generate a number of parameters which can be used to quantify the BE.

2.2.1 Stress related parameters

The most straightforward of these has been termed the *Bauschinger stress*, $\Delta\sigma$ [24], and is given as:-

$$\Delta\sigma = \sigma_F + 0.2\%\sigma_R \qquad \ldots\ldots 2.1$$

If $\Delta\sigma$ has a value of 0, then clearly no Bauschinger effect exists, ie when $0.2\%\sigma_R = -\sigma_F$, Figure

6. However, it should be stressed that the selection of $0.2\%\sigma_R$ to characterise the reverse curve is purely arbitrary, and some other strain offset may be more suitable.

Another frequently quoted parameter is the *Bauschinger Stress Parameter*, β_σ [24], defined as:-

$$\beta_\sigma = \Delta\sigma/\sigma_F \qquad \ldots\ldots 2.2$$

$$= (\sigma_F + 0.2\%\sigma_R) / \sigma_F$$

$$= 1 + (0.2\%\sigma_R/\sigma_F)$$

This parameter has a minimum value of 0 where the Bauschinger effect is not observed and a theoretical maximum value of 2, if reverse yielding occurs immediately after stress reversal, ie when $0.2\%\sigma_R = \sigma_F$, Figure 6.

Whilst each of these stress related parameters is useful in characterising the BE, in that they provide data of physical significance which is relatively easy to interpret, they have the disadvantage of relying upon $0.2\%\sigma_R$ to characterise the reverse flow stress curve. Wilson and Bate [25], who aged spheroidised 1.1%C steel specimens after prestraining to restore a reverse yield point, used $0.3\%\sigma_R$ in their calculations as this gave a better estimate of reverse yield stress than $0.2\%\sigma_R$, but the applicability of this finding to Q2N has yet to be verified. Naval Engineering Standard 826 [10] however, stipulates that in the absence of a yield point the 0.2% proof stress should be measured, although this only applies to the tensile properties of Q2N in its quenched and tempered conditions.

2.2.2 Strain related parameters

In order to overcome this difficulty of accurately chatacterising the reverse flow curve, a series of *strain* related parameters has also been developed to characterise the Bauschinger effect, because the strain at which a particular event occurs can often be just as informative as the

corresponding stress.

The first of these, the *Bauschinger strain*, ϵ_1, [24] is defined as the amount of reverse strain required to achieve a reverse stress of $-\sigma_F$, after the application of a prestress of $+\sigma_F$, Figure 7. It has a value of 0 where no BE exists. It also has the advantage that it can be measured without reference to a reverse yield event, and can therefore be determined more accurately than the preceding stress related parameters.

The *Bauschinger strain parameter*, β_ϵ, is also commonly quoted and is defined as:-

$$\beta_\epsilon = \epsilon_1 / \epsilon_P \qquad \ldots\ldots 2.3$$

and has a minimum value 0 when the BE is not observed and a maximum theoretical value of 2, but is usually found to range from 0.5 to 1.5 [24], Figure 7.

2.2.3 Energy related parameters

Whilst the stress and strain related Bauschinger parameters can provide useful information about the BE displayed by a particular material, they are not able to characterise it completely. For example, Abel & Muir [24] showed that a fully-killed low carbon steel, which exhibited a β_σ value of 1.6 indicative of a large BE, also possessed a β_ϵ value of 0.5 which is symptomatic of a smaller BE. This apparent dichotomy has led to the development of the *Bauschinger energy parameter*, β_E, which takes into account the overall shape of the reverse stress curve [24] where :-

$$\beta_E = E_S/E_P \qquad \ldots\ldots 2.4$$

The *Bauschinger energy*, E_S, represents the additional energy that would have been required to achieve a reverse plastic strain equal to the Bauschinger strain, had the material in question

behaved in a 'perfectly plastic' fashion, exhibiting neither the BE nor any work hardening, whilst E_P represents the energy associated with achieving a prestrain of ϵ_P, Figure 8.

Where no BE exists $E_S = 0$ and a zero value of β_E must be recorded. It also has an upper limit of 1 when $E_S = E_P$, assuming that E_S can never be greater than the energy put into a specimen during prestraining, E_P, and usually ranges from 0.1 to 0.5.

To summarise, the following are the Bauschinger parameters most frequently quoted in the literature:-

Stress related parameters	Strain related parameters	Energy related parameters
Primary Bauschinger Parameters		
$\Delta\sigma$ - The Bauschinger stress.	ϵ_1 - The Bauschinger strain.	E_S - The Bauschinger energy.
Secondary Bauschinger Parameters		
β_σ - The Bauschinger Stress Parameter.	β_ϵ - The Bauschinger Strain Parameter.	β_E - The Bauschinger Energy Parameter.

The first parameter within each of the above classifications ($\Delta\sigma$, ϵ_1 and E_S) are referred to as *primary Bauschinger parameters* (PBP), as they all express a specific quantity in terms of their respective units, ie $\Delta\sigma = 100$MPa, $\epsilon_1 = 2\%$ and $E_S = 5$ MJ/m^3, and have a value of zero where no BE is observed. The second parameter within each classification (β_σ, β_ϵ and β_E) is known as a *secondary Bauschinger parameter* (SBP), and is dimensionless. Values range between a lower limit of 0, where no BE exists, and an upper limit of 2 for β_σ and β_ϵ, or 1 in the case of β_E, when the BE is at its theoretical maximum.

Where specific information about the BE exhibited by a particular material is required, during the design stage of a submarine for example, PBP data may be more useful.

However, during the preceeding research phase, SBP data may prove to be more helpful as a comparative tool, in determining the effect of heat treatment on the BE exhibited by Q2N for example. Todate, whilst some work on the effect of tensile prestrain on the 0.2% compressive proof stress of Q2N has been reported [9]and indicates that the reduction in $0.2\%\sigma_R$ reaches

saturation after a tensile prestrain of approximately 0.5%, Figure 9, its BE has yet to be fully characterised.

2.3 The Bauschinger effect in pure metals and single phase alloys

The principal advantage of studying the BE in pure metals and single phase alloys, is that various aspects of it can be examined without the need to take into account the influence of a second phase, although the difficulty of comparing the BE displayed by more complex materials still remains.

In an attempt to resolve this problem Tadashi *et al* [4] have developed a *unified approach* to the BE, the essence of which is presented in Figure 10. Figure 10a shows five reverse true stress / strain curves, ϵ_r vs (σ / σ_P), exhibited by aluminium, each associated with a different level of tensile prestress, σ_P. However, when the same data are re-plotted in the form of (ϵ_r / σ_P) vs (σ / σ_P) curves , Figure 10c, it can be seen that all five curves are virtually coincident, the implication being that the BE exhibited by aluminium can be represented by a single unified curve, defined by the equation:-

$$\sigma / \sigma_P = K.f_n (\epsilon_r / \sigma_P) \qquad \ldots\ldots 2.5$$

K = constant : f_n = 'a function of'

The same is also true of copper , Figures 10b & d.

The line ABC in Figures 10c & d represents the unified curve for a perfectly plastic material which does not exhibit the BE, and the further the unified curve for a particular material deviates from this line the greater the BE it exhibits. Consequently, when the true stress/strain curves for copper and aluminium are normalised with respected to σ_P and superimposed, Figure 11, it can be seen that the unified curve for copper lies further to the left than that of aluminium, indicating that copper exhibits a slightly greater BE than aluminium.

The concept of a unified curve can also be used to monitor changes in the BE exhibited by a

particular material, in response to any microstructural modifications. Figure 12a, for example, shows that increasing the grain size of aluminium from 71μm to 440μm has virtually no effect on the shape or position of its unified curve, demonstrating that grain size has little influence on the BE exhibited by aluminium. The same is again true for copper, Figure 12b.

The effect of temperature on the BE is somewhat different. Figures 12c & d show that for aluminium and copper, an increase in test temperature results in a shift of its unified curve to the right, indicating a reduction in the BE with increasing temperature.

It should be stressed that the above trends are applicable only to aluminium and copper. Whether the unified approach can be applied to Q2N is not yet clear, as Tadashi's analysis focused primarily on single phase metals which form a three dimensional dislocation cell structure during plastic deformation. Although the dislocation arrangement formed by Q2N is unknown, and a unified curve for Q2N has not yet been derived, it could be useful as a comparator for the BE in other cheaper steels of a similar strength level to Q2N such as HSLA 100 and NSS 550.

2.4 The Bauschinger effect in two phase alloys

Two phase alloys generally exhibit a much greater BE than single phase alloys. This can be seen more clearly in Table 2 where the permanent softening, as a percentage of the applied prestress, exhibited by the single phase alloys Al-3%Mg (solid solution) and decarburized steel at approximately 15%, is considerably less than the 30% - 40% associated with two phase materials, such as precipitation hardened Duralumin or a 1.1%C steel containing a fine dispersion of cementite particles [19].

However, the presence of a second phase is not always a guarantee of a large BE. This can be seen more clearly in Figure 13a, which shows the effect of ageing time on the shear yield strength (τ_Y) and permanent softening $(\tau_S)_3$ exhibited by solution treated Al-4%Cu. In its *as quenched* condition, the permanent softening exhibited by this alloy, at approximately 60 M Pa, is quite

small and is consistent with it being a single phase material. However, after being aged at 195°C for 10 hours , Figure 13a clearly demonstrates that whilst the shear yield strength, (τ_Y), of Al-4%Cu increased from 210 M Pa to almost 350 M Pa, in response to the sequential precipitation of GP zones and θ" particles, a corresponding increase in permanent softening , (τ_S)$_3$, was not recorded. As ageing proceeds (τ_Y) continues to increase as θ" particles are progressively replaced by θ' particles until it reaches a maximum of 350 MPa after approximately 30 hours while (τ_S)$_3$ is seen to rise to 200 MPa. After 300 hours (τ_Y) has decreased to 300 MPa due to over ageing whilst (τ_S)$_3$ reaches a maximum of 340 MPa, in association with a microstructure containing a dispersion of θ' platclcts. This demonstrates that the mechanisms involved in the forward strengthing of Al-4%Cu are not coincident with the BE and permanent softening exhibited by this alloy, and that the BE in two phase alloys may also be dependant upon the nature of the second phase, and more specifically on its resistance to plastic deformation. The GP zones and θ" precipitates mentioned in the preceding example are coherent with the matrix which surrounds them and can be sheared by dislocations, whilst the θ' platelets which are semi-coherent are much harder to shear and are therefore associated with a larger BE. This behaviour has also been observed in other precipitation hardened materials such as the Al-Cu-Mg-Fe-Si alloy 2024, Figure 13b. When this alloy is aged so that it contains shearable GPB zones (2024-T4) it exhibits a Bauschinger strain of 0.1% after a prestrain of 1%. However, when 2024 is aged so that it contains non-shearable S' (Al_2CuMg) precipitates (2024-T6) it displays of much larger Bauschinger strain of 0.8% for the same prestrain.

The magnitude of the BE is also influenced by the distribution of the second phase. For example, Wilson *et al* found that the permanent softening , as a percentage of applied prestress, exhibited by a 0.74%C steel which had been quenched and tempered to give a fine dispersion of carbides was 35%. However, that displayed by a sample of the same material, which had been

spheroidised to generate a coarser distribution of carbides, was lower at 29% implying that the finer the distribution of carbides/second phase, the greater the BE,[19].

To summarise therefore, a material which can be modelled as a soft, plastically deformable matrix containing a fine dispersion of hard, non-shearable second phase particles, would normally be expected to exhibit a sizeable BE.

2.5 Modelling the Bauschinger effect

The above description of a material comprising of a soft matrix containing hard particles is applicable to Q2N, which is essentially a matrix of martensite containing a fine dispersion of carbides, and is thus amenable to analysis by the *parallel elements model* (PEM) of Masing, [26]. This approach considers a composite specimen comprising of two perfectly plastic elements P and M, in parallel, Figure 14, where the tensile yield strength of P, σ_{YP}, is considerable larger than that of M, σ_{YM}. To simplify the analysis, it is assumed that P and M have the same elastic modulus and volume fraction, ie 50% P and 50% M. On loading in tension, Figure 14a, the elastic portion of the stress/strain curves for P and M will initially be coincident up to a stress σ_{YM}. At this stress M will start to deform plastically whilst P will continue to behave elastically. At the point where P is just about to yield, σ_{YP}, the stress in M is still σ_{YM} and the externally applied stress needed to reach this position, σ_F, is given by $\sigma_{YM} + f_n(\sigma_{YP} - \sigma_{YM})$, where $f_n = '$ a function of '.

If the composite specimen is then unloaded so that $\sigma_F = 0$, Figure 14b, the stress in P drops to $(\sigma_{YP} - \sigma_F)$, and is balanced by a compressive stress in M of $-f_n(\sigma_{YP} - \sigma_{YM})$.

If the composite specimen is then load compressively, Figure 14c, the tensile stress in P will decrease, whilst the compressive stress in M will continue to increase until it reaches $-\sigma_{YM}$, when M will start to deform plastically. At this point the composite specimen will also yield but at a stress $\sigma_R = [-\sigma_{YM} + f_n(\sigma_{YP} - \sigma_{YM})]$. If no BE existed the composite specimen would yield

in compression at $-\sigma_{YM}$. Consequently, since $|-\sigma_{YM} + f_n(\sigma_{YP} - \sigma_{YM})| < |-\sigma_{YM}|$ the PEM, as a continuum model, has been able to predict a reduction in compressive yield strength in response to a tensile prestrain, ie the BE , without reference to dislocation interaction mechanisms.

The PEM also accounts for permanent softening, $\Delta\sigma_P$, as follows:-

$$\begin{aligned}\Delta\sigma_P &= \sigma_F + \sigma_R \\ &= [\sigma_{YM} + f_n(\sigma_{YP} - \sigma_{YM})] + [-\sigma_{YM} + f_n(\sigma_{YP} - \sigma_{YM})] \\ &= 2f_n(\sigma_{YP} - \sigma_{YM}) \qquad \ldots\ldots 2.6\end{aligned}$$

This assumes that f_n is not affected by the reversal of the direction of deformation.

and concludes that its magnitude is twice that of the stress in M, the weaker element, after the applied prestress , σ_F , has been removed. The Atkinson, Brown, Stobbs (ABS) model however [5], has shown that for Cu-SiO_2 values of $f_n(\sigma_{YP} - \sigma_{YM})$ which they denoted as $\langle \sigma^F \rangle_M$, can be derived theoretically from the following equation:-

$$\langle \sigma^F \rangle_M = 2\mu f\gamma\epsilon_P^*\mu^*/[\mu^* - \gamma(\mu^* - \mu)] \qquad \ldots\ldots 2.7$$

where μ is the shear modulus of the matrix; μ^* is the shear modulus of the particles; γ is an accommodation factor; f is the volume fraction of particles and ϵ_P^* is the strain experienced by the particles during prestraining, and from Equ 2.6 it follows that :-

$$\begin{aligned}\Delta\sigma_P &= 2f_n(\sigma_{YP} - \sigma_{YM}) \\ &= 2\langle \sigma^F \rangle_M \\ &= 4\mu f\gamma\epsilon_P^*\mu^*/[\mu^* - \gamma(\mu^* - \mu)] \qquad \ldots\ldots 2.8\end{aligned}$$

Therefore, provided suitable values for the variables in Equ 1.8 can be found it should be possible to derive theoretical values of $\Delta\sigma_p$ as a function of prestrain for comparison with those measured experimentally. The shear modulus of Q2N, μ , can be determined from its Young's modulus, E = 210GPa , and the Poisson's ratio, $\nu = 0.29$ [27], ie

$$\mu = E / 2(1 + \nu) \qquad \ldots\ldots 2.9$$

which yields a value for μ_{Q2N} of 81.4GPa.

The volume fraction of carbides in Q2N , f , which are a mixture of Mo_2C, Cr_3C_2 and Fe_3C is more difficult to determine but a value ranging from 0.016 to 0.024 is typically quoted [28], whilst a value of 0.5 for the accommodation factor, γ , associated with these carbides is appropriate [2], assuming they are spherical and behave elastically.

The shear moduli , μ^* , of Mo_2C and Cr_3C_2 are 96 G Pa and 132GPa respectively, [29], whilst that of Fe_3C is unknown. If μ^* is taken as 96GPa then the quotient $(\mu^*/ (\mu^* - \gamma(\mu^* - \mu_{Q2N})))$ has a value of 1.08 which increases to 1.24 if μ^* equals 132GPa.

When each of these values are substituted into Equ 2.8, a predictive equation for the permanent softening exhibited by Q2N, $\Delta\sigma_p^{Q2N}$, as a function of tensile prestrain, ϵ_p , can be given as :-

$$\Delta\sigma_p^{Q2N} = 38(\pm 10) \times \epsilon_p \qquad \ldots\ldots 2.10$$

Units: $\Delta\sigma$ [MPa] : ϵ_p [%]

$$\mu_{Q2N} = 81.4\text{GPa} : f = 0.016 \rightarrow 0.024 : \gamma = 0.5 : \mu^* = 96\text{GPa} \rightarrow 132\text{GPa}$$

Consequently, since the largest strain experienced by Q2N plate and T-bar during fabrication is in the order of 10%, theoretically it should not exhibit a permanent softening in excess of

380±100MPa , which is approximately 55%±15% of its minimum 0.2% tensile proof strength of 690MPa. This indicates a potentially serious problem theoretically, and the main purpose of the present investigation is to establish experimentally whether the theoretical predictions are sound.

CHAPTER 3

EXPERIMENTAL PROCEDURE

3.1 Research strategy

The literature survey has highlighted a number of important points, which are applicable to characterising the BE exhibited by Q2N, a steel with a microstructure of tempered martensite containing a fine dispersion of carbide particles. These include the importance of test type, the significance of terms used to describe the BE and the possibility of a unified curve for its characterisation. These aspects are now considered in more detail.

Firstly, as Q2N is principally intended to be used in the form of heavy gauge plate with a thickness of at least 25mm the PSS test, used for determining the BE in thin sheet material, is of little relevance. Also, the large amounts of deformation associated with the RT test are not particularly advantageous when investigating Q2N, as its elongation during tensile testing is limited to approximately 25%. The uniaxial tension/compression (TC) however, where a specimen is initially plastically deformed in tension by a specified prestrain, ϵ_P, or prestress, σ_F, at which point the direction of deformation is reversed, and testing is completed by plastically deforming it in compression, is suited to studying the BE in Q2N as the strain range over which it operates, ±10%, is coincident with the strains experienced by Q2N plate and T-bar sections whilst being rolled to submarine pressure hull radius.

In addition to it being the most widely adopted test procedure, suitable mechanical testing equipment was available.

When Q2N is prestrained in tension beyond about 10%, it starts to develop regions of localised plastic deformation, and any subsequent compressive loading then becomes impossible due to problems of alignment resulting in the onset of buckling. Similarly, the maximum compressive strain that can be achieved during testing before buckling occurs is also limited to approximately

10%. Consequently, the level of tensile prestrain investigated was restricted to approximately 8%, and compressive loading was stopped as soon as buckling occurred. Buckling effects were reduced by the selection of an 'hourglass' shaped TC test specimen, Figure 15, which had a parallel sided central gauge section with a diameter and gauge length of 12.5mm.

Secondly, most experimental work has concentrated on describing the BE in terms of stress alone. Whilst such data can be extremely useful they can also be misleading, because of the difficulty associated with the accurate location of a reverse yield point. Q2N, for example, does not exhibit a compressive yield point after being prestrained in tension, and it is necessary to use the 0.2% compressive proof stress, $0.2\%\sigma_R$, as a measure of reverse yield strength. However, the strain and energy related BE parameters can be measured without reference to a reverse yield event, and can therefore be determined more accurately. Consequently, each of the parameters highlighted in Chapter 2 (list below) are also used in the present work to comprehensively characterise the BE exhibited by Q2N.

Stress related parameters	Strain related parameters	Energy related parameters
Primary Bauschinger Parameters		
$\Delta\sigma$ - The Bauschinger stress.	ϵ_1 - The Bauschinger strain.	E_S - The Bauschinger energy.
Secondary Bauschinger Parameters		
β_σ - The Bauschinger Stress Parameter.	β_ϵ - The Bauschinger Strain Parameter.	β_E - The Bauschinger Energy Parameter.

Thirdly, the possibility of characterising the BE by a single *unified* curve has also been highlighted. Todate, this unified approach has been only applied to single phase materials and whether such an analysis is applicable to Q2N is not yet clear. In an effort to clarify this situation an attempt has been made here to construct such a curve specifically relating to Q2N.

Finally, it was also suggested that the *parallel elements model* (PEM) in combination with the ABS model may be capable of predicting the permanent softening , $\Delta\sigma_P$, exhibited by Q2N as a function of tensile prestrain. This was on the assumption that Q2N can be modelled as a

composite material, with a perfectly plastic matrix containing a fine dispersion of hard second phase particles. Theoretical and experimental values of $\Delta\sigma_p$ for Q2N are presented here and an evaluation of the applicability of this model to Q2N is also given.

3.2 Experimental detail

3.2.1 Overview of experimental procedure

Fourteen TC test specimens were taken from the longitudinal direction of a 25mm thick Q2N plate identified as No.7483 , and labelled 7483/1 through to 7843/14, Figure 16. Each specimen was prestrained in tension at a strain rate of 5×10^{-5} s^{-1} by amounts ranging from 0.25% to 8.1%, and then subjected to compressive loading which was stopped when buckling was visually observed. Testing was carried out at room temperature (18°C) using an ESH servohydraulic mechanical testing machine capable of applying a load of ±250kN, Figure 17. Strains were measured using a SANDNER 10-5X extensometer with a range of ±20%, Figure 18, and a strain rate of 5×10^{-5} s^{-1} was selected as being representative of that reported in the literature. .

3.2.2 Alignment of mechanical testing equipment

The alignment of the loading train was checked by testing a TC specimen, fitted with four strain gauges located at the 90°, 180°, 270° and 360° positions around the circumference of its gauge length, Figure 19. This specimen was deformed *elastically* in tension and compression. Figure 20 shows that the tensile and compressive elastic moduli had an average value of 209.5±1.8GPa, and varied by less than 1% irrespective of the location of the strain gauges or the direction of testing, indicating that alignment was better than a 5% variation in moduli which is normally considered to be acceptable [30].

3.2.3 Extensometer calibration

Prior to testing, the SANDNER 10-5X extensometer, which had a gauge length of 10mm, was calibrated using the displacement calibration device shown in Figure 21. This consisted of two

aligned rods to which the extensometer was attached, with a separation that was controlled by a micrometer located at one end. This micrometer was accurate to ±0.5μm and enabled the extensometer to be calibrated to give an output of 1volt per 1mm extension, accurate to ±1μm over a strain range of ±20%.

3.2.4 Mechanical Testing Procedure

Prior to testing, the diameter of the central gauge length of each TC specimen was measured 3 times using a digital micrometer, accurate to ±0.5μm, Figure 22a, and then a circular collar produced from HY130 steel was screwed on to one end of the specimen, Figure 22b. The internal thread of the collar and the external thread of the specimen were machined to a close tolerance to ensure a tight fit , thereby minimising the possibility of movement / misalignment during testing. This assembly was then placed in to the lower loading ram of the ESH machine which had been designed to accept the outer diameter of the collar, Figure 22c. Again the internal diameter of the ram and the external diameter of the collar were machined to a close tolerance to ensure a tight fit. A circular restraining cap with a 25mm hole drilled through its centre, also produced from HY130, was then placed over the specimen and screwed on to the outer diameter of the lower loading ram until its lower surface contacted the upper surface of the collar. The cap was then hand tightened thus securing the collar / specimen assembly in to the lower loading ram, Figure 22d. A second cap was then placed over the specimen in the up side down position and another collar was screwed to the remaining threaded end of the specimen, Figure 22e. The upper loading rod of the ESH machine was then hydraulically lowered to accepted this collar, Figure 22f, which was then fastened in place by screwing the second restraining cap on to the outer diameter of the upper loading rod, Figure 22g, thus firmly securing the entire specimen within the servohydraulic testing machine. The SANDNER 10-5X extensometer was then attached to the central gauge length of the specimen using 2 small restraining springs, and the separation of its arms was set at

10mm using a calibrated gauge block, Figure 22h.

The specimen was then prestrained in tension, Figure 22i, by slowly lowering the lower loading ram at a velocity sufficient to induce at strain rate of 5×10^{-5} s^{-1} across the gauge length of the specimen. The displacement of the lower loading ram was restricted to ±5mm to avoid exceeding the safe operating range of the extensometer which was ±5mm. The load range used during testing was set at ±250kN and was recorded by a load cell located immediately above the upper loading rod.

After the required level of tensile prestrain had been reached the direction of loading was reversed and the specimen was unloaded, Figure 22j, and then tested in compression until buckling was observed, Figure 22k. After buckling the extensometer was removed, the specimen was unloaded and then removed from the testing machine by unscrewing both restraining caps and raising the upper loading rod.

The output of the extensometer and the load cell were recorded on an X-Y chart recorder, the X-axis of which was calibrated to given full scale deflection (FSD) of ± 1mm extension whilst its Y-axis was set to given a FSD of ±125kN. The resulting load vs extension chart, Figure 23, was then used to calculate the BE parameters mentioned previously. An example of these calculations is presented in Annex A.

3.2.5 TC specimen stress distribution

A Vickers hardness survey of material taken from the gauge length and one of the threaded ends of a TC specimen which had received a prestrain of 8% is presented in Figure 24, and shows that the hardness of deformed gauge length material was 277±4 whereas that of undeformed material from the end of the specimen was 264±4. A standard deviation of ±4 in the hardness of deformed material also demonstrates that the stress distribution within the specimen during deformation was uniform.

CHAPTER 4

RESULTS

4.1 Introduction

The aim of this chapter is to present the results arising from the experimental testing program undertaken to study the BE in Q2N, detailed in Chapter 3. The opening section describes the effect of prestrain on the stress, strain and energy related BE parameters, then examines the correlation between experimental and theoretically derived values of the permanent softening exhibited by Q2N, and concludes by addressing the feasabiltiy of characterising the BE in Q2N by a *single* unified curve.

4.2 Experimental data and bauschinger effect parameters

The engineering σ/ϵ curves for all TC specimens are shown in Figure 25, whilst the associated true σ/ϵ curves, required for the determination of the permanent softening exhibited by Q2N, calculated on the assumption of constant volume are presented in Figure 26. Values of each of the BE parameters selected for investigation at each levels of prestrain are shown in Table 3, and an example showing the measurement of experimental values and the calculation of BE parameters for a prestrain of 5.1% is presented in Annex A.

4.3 The effect prestrain on banschinger effect parameters

4.3.1 Stress related parameters

From Figure 27a it can be seen that there is a gradual decrease in $0.2\%\sigma_R$ with increasing level of prestrain. The 0.2% compressive proof stress, $0.2\%\sigma_R$, of Q2N after a tensile prestrain of 8.1% was 398MPa. This represents a reduction of almost 50% when compared with a $0.2\%\sigma_R$ of 757MPa for material which had not been prestrained, indicating that Q2N exhibits a significant BE. Figure 27b shows that the Bauschinger stress, $\Delta\sigma$, increased from 264MPa after a 0.48% prestrain up to 434MPa after a prestrain of 7.85% demonstrating that the magnitude of the BE

exhibited by Q2N was proportional to the applied prestrain and is characterised by the equation:

$$\Delta\sigma = 19.3(\pm 2.8)\epsilon_p + 285(\pm 23) \quad \ldots\ldots 4.1$$

Units: $\Delta\sigma$ [MPa] : ϵ_p [%] : Range: ϵ_p 0.48% → 8.1% : Equation determined by linear regression

The Bauschinger stress parameter, β_σ , also increased from 0.363 to 0.522 over the same prestrain range, Figure 27e, illustrating that the magnitude of the BE exhibited by Q2N, relative to the applied prestress, was also proportional to prestrain and is characterised by the equation:

$$\beta_\sigma = 0.017(\pm 0.004)\epsilon_p + 0.39(\pm 0.02) \quad \ldots\ldots 4.2$$

Units: ϵ_p [%] : Range: ϵ_p 0.48% → 8.1% : Equation determined by linear regression

4.3.2 Strain related parameters

From Figure 27c it can be seen that the Bauschinger strain, ϵ_1 , increased from 0.82% up to 6.4% as the applied prestrain increased from 0.48% up to 8.1% confirming that Q2N exhibited the BE. Because ϵ_1 has value of zero where no BE exists, it also demonstrates that the magnitude of the BE exhibited by Q2N increased proportionally with increasing prestrain in accordance with the following equation:

$$\epsilon_1 = 0.86(\pm 0.02)\epsilon_p \quad \ldots\ldots 4.3$$

Units: ϵ_1 [%] : ϵ_p [%] : Range: ϵ_p 0.48% → 8.1% : Equation determined by linear regression

However, the Bauschinger strain parameter, β_ϵ , decreased assymtopically from a value of 1.7 with increasing prestrain, Figure 27f, and appeared to be constant at ≈0.8 after a prestrain of approximately 5%. This indicates that the magnitude of the BE exhibited by Q2N, relative to the applied prestrain, decreased in a non-linear manner with increasing prestrain in accordance with the following equation:

$$\beta_\epsilon = 1.2 \exp^{-0.7\epsilon p} + 0.8 \quad \ldots\ldots 4.4$$

Units: ϵ_p [%] : Range: c_p 0.48% → 8.1%

4.3.3 Energy related parameters

Figure 27d shows that the Bauschinger energy, E_S, increased proportionally from 1.2 MJ/m^3 after a 0.48% prestrain up to 7.2 MJ/m^3 after a prestrain of 7.85%, illustrating once again that Q2N exhibited the BE, the magnitude of which increased with prestrain in accordance with the following equation:

$$E_S = 0.703(\pm 0.07)\epsilon_P + 1.34(\pm 0.6) \quad \ldots\ldots 4.5$$

Units: E_S [MJ/m^3] : ϵ_P [%] : Range: ϵ_P 0.48% → 8.1% : Equation determined by linear regression

The Bauschinger energy parameter, β_E, however decreased assympotically from a value of 0.33 with increasing prestrain, Figure 27g, becoming constant at ≈0.1 after a prestrain of approximately 5%. This demonstrates that the magnitude of the BE exhibited by Q2N, relative to E_P, also decreased non-linearly with increasing prestrain and was characterised by the equation:

$$\beta_E = 0.3 \exp^{-0.8\epsilon p} + 0.12 \quad \ldots\ldots 4.6$$

Units: ϵ_P [%] : Range: ϵ_P 0.48% → 8.1%

4.3.4 Permanent softening

From Figure 25 it can be seen that for any particular engineering prestrain the reverse compressive engineering σ/ϵ curve never becomes parallel with the forward tensile curve. In fact, the reverse curve intersects the forward curve implying that permanent hardening is occurring. This effect disappears however when the true σ/ϵ curves associated with each level of prestrain are examined and permanent softening is observed Figure 28. This is because, whilst the difference between engineering and true stress for strains of less than 1% is small, at larger strains the difference becomes quite significant and is larger than the permanent softening effect itself. Consequently, when measurements of the permanent softening, $\Delta\sigma_P$, exhibited by Q2N were obtained from true σ/ϵ curves, Figure 26, it can be seen that $\Delta\sigma_P$ increased linearly with increasing prestrain, Figure 29a, and is characterised by the following equation:

$$\Delta\sigma_P^{Q2N} = 24.5(\pm 0.6)\epsilon_P \quad \ldots\ldots 4.7$$

Units: $\Delta\sigma_P$ [MPa] : ϵ_P [%] : Range: ϵ_P 0.25% → 8.1% : Equation determined by linear regression

Theoretical values of $\Delta\sigma_P$ for Q2N derived from Equ. 2.10 are presented in Figure 29b in conjunction with values determined experimentally, and shows that experimental values of $\Delta\sigma_P$ were approximately 35% less than those predicted by the ABS model.

4.3.5 Unified curve

The reverse engineering and true σ/ϵ curves presented in Figures 25 & 26 are replotted in Figures 30 & 31, with both axis being normalised with respect to the applied prestress, σ_P, in order to conform with the *unified* approached adopted by Tadashi *et al* [4]. From Figures 30 & 31 it can be seen that these *unified* curves are not coincident. Consequently, the BE exhibited by Q2N can not be represented by a single *unified* curve.

CHAPTER 5

DISCUSSION

5.1 Review of results

The aim of this chapter is to explore more fully the experimental results presented in Chapter 4, with particular attention being paid to the practical significance of these results on the integrity of submarine pressure hulls and other large fabricated structures. Shortcomings in the ability of the ABS/PEM models to accurately characterise the BE exhibited by Q2N are addressed, and the applicability of the *unified* approach to Q2N is also considered.

5.2 Primary Bauschinger effect parameters

From Figures 27b, c & d it can be seen that each of the *primary* BE parameters ($\Delta\sigma$, ϵ_1 and E_S) increased linearly with increasing prestrain. As they have a value of zero where no BE exists, it is evident that Q2N does exhibit the BE. Whilst this may appear to be an obvious statement to make, it is also one of fundamental importance. For example, it has been calculated that the BE may be responsible for a reduction of about 20% in the ultimate bending strength of the pressure hull of a submarine fabricated using Q2N [13]. The BE is also likely to play an important role in the structural integrity of other large steel fabrications such as oil rigs, bridges, chemical industry pressure vessels etc, although the extent of its influence in these applications has yet to be fully characterised as the significance of the BE has yet to be recognised by the wider engineering community.

In addition, Figures 27b, c & d show that the magnitude of the BE exhibited by Q2N, assessed in terms of stress, strain and energy, was proportional to the applied prestrain. Although the Bauschinger stress, $\Delta\sigma$, increased to 431MPa after a prestrain of 8.1%, this may not be an accurate measure of its true magnitude, because of the necessity of using $0.2\%\sigma_R$ as a measure of reverse yield strength, due to the absence of a discrete yield point during reverse loading.

However, the Bauschinger strain, ϵ_1 , which increased to 6.4% after a prestrain of 8.1%, was considered to be an accurate measure of the BE exhibited by Q2N, because it can be determined without reference to a reverse yield event. The same is also true of the Bauschinger energy, E_S , which increased to 5.9 MJ/m^3 after a similar prestrain.

Wilson and Bate [25], who aged spheroidised 1.1%C steel specimens at 200°C for 30 minutes after prestraining to restore a reverse yield point, Figure 32, used $0.3\%\sigma_R$ in their calculations as this gave a better estimate of reverse yield stress than $0.2\%\sigma_R$ (cf. 2.2.1). The $0.3\%\sigma_R$ of Q2N after a prestrain of 5.1% was -466MPa (as opposed to a $0.2\%\sigma_R$ of -436MPa) which gives a Bauschinger stress, $\Delta\sigma$, of 345MPa and a value for the Bauschinger stress parameter, β_σ , of 0.43, which are 7% - 9% lower than values for these parameters calculated using $0.2\%\sigma_R$. If $0.3\%\sigma_R$ does characterise the reverse flow stress curve for Q2N better than $0.2\%\sigma_R$, this would imply that values of $\Delta\sigma$ and β_σ recorded here are artificially high.

To determine whether this effect is applicable to Q2N, a TC specimen was prestrained in tension by 5.1% and heat treated at 200°C for 30 minutes, before being tested in compression. Figure 33 shows that this specimen did not exhibit a distinct reverse yield point, although it should be noted that the $0.2\%\sigma_R$ of Q2N heat treated in this way at 491MPa, was approximately 13% higher than the $0.2\%\sigma_R$ of unheat treated material. Figure 33 also demonstrates, that whilst the compressive σ/ϵ curve for prestrained Q2N did not develop a recognisable yield point in response to this strain ageing treatment, a region of elastic deformation during the early stages of reverse straining was restored, which is absent from the compressive σ/ϵ curve of material which was not aged.

From Table 3 it can also be seen that the Bauschinger stress, $\Delta\sigma$, and the Bauschinger strain, ϵ_1 , exhibited by strain aged Q2N at 320MPa and 3.95% repectively, were approximately 15% lower than values for these parameters associated with unheat treated material. The effect of strain ageing on the Bauschinger energy, E_S, displayed by Q2N was even more pronounced, being

reduced by more than 25%, implying that the BE exhibited by Q2N can be reduced by a simple low temperature heat treatment, although the ramifications of this finding have yet to be fully investigated.

5.3 Secondary Bauschinger effect parameters

From Figures 27e, f & g, which show the effect of prestrain on the *secondary* BE parameters β_σ ,β_ϵ and β_E , it can be seen that whilst the Bauschinger stress parameter, β_σ , increased linearly with increasing prestrain, the Bauschinger strain parameter, β_ϵ , and the Bauschinger energy parameter, β_E , both decreased assymtopically with prestrain. This complex pattern of behaviour can be better understood if the secondary BE parameters are interpreted as indicating the extent of the BE as a fraction of its theoretical maximum.

For example, after a prestrain of 6.97%, Q2N displayed a Bauschinger strain parameter, β_ϵ , of 0.86. Because this parameter has a minimum value of 0 and an upper limit of 2 (cf 2.2.2), this particular value of β_ϵ is indicative of a BE with a magnitude of approximately 43%, relative to its theoretical maximum and should be regarded as being significant but not excessive.

The same argument can also be applied to the Bauschinger stress parameter, β_σ , and the Bauschinger energy parameter, β_E , which both have a minimum value of 0 and an upper limit of 2 and 1 respectively. At the level of prestrain used in the preceding example, β_σ and β_E had values of 0.511 and 0.116 respectively, indicating that the magnitude of the BE exhibited by Q2N determined from stress related parameters was approximately 26% of its theoretical maximum, whilst that derived from energy related parameters at 11.6% was considerable lower.

Consequently, the data presented in Figures 27e, f & g can be reinterpreted as showing that whilst the magnitude of the BE exhibited by Q2N derived from stress related parameters, β_σ , **increased** with prestrain relative to the maximum theoretical value of β_σ (Equ 4.2), its magnitude **decreased** assymtopically with prestrain, relative to the maximum theoretical values

of β_ϵ & β_E, (Equs 4.4 & 4.6) when assessed in terms of the strain and energy related parameters. This apparently contradictory behaviour has also been reported by Abel & Muir [24], Figure 34, for a low carbon mild steel. They attributed the increase in β_o with prestrain to the propagation of a Luders front during the prestraining of their specimens. As Q2N does not plastically deform by this mechanism it seems unlikely that Abel and Muir's explanation for the increase in β_o with prestrain applies, although it clearly demonstrates that if the BE is to be fully characterised, it must be classified not only in terms of stress related parameters, but also with respect to strain and energy related parameters.

5.4 Modelling the Bauschinger effect

Although experimental values for the permanent softening exhibited by Q2N, $\Delta\sigma_P$, were approximately 35% less than values predicted by the PEM/ABS model (Equ 2.10), adopting the lower bound of equation 2.10 reduces this discrepancy to approximately 13%. However, for prestrains below 1% the difference between experimental and theoretical values of $\Delta\sigma_P$ is less than 5MPa and is well within the experimental error. This close agreement between theory and experiment for small prestrains has also been reported by Atkinson *et al* [2], Figure 35.

For prestrains above 1% the difference between experimental and theoretical lower bound values of $\Delta\sigma_P$ starts to increase reaching a value of 40% after a prestrain of 7.85%. This has been attributed to a breakdown in the elastic particle / plastic matrix interface [31], Figure 36 , thereby violating one of the preconditions of the PEM, that both elements are intimately bonded and will therefore always experience the same level of strain. It should also be noted that the PEM assumes that the elastic element exists in the form of a discrete block of material. However, the hard, elastic carbides in Q2N are extremely small (~ 0.1μm in diameter) and have a very fine distribution, which may also contribute to the discrepancy between theoretical and experimental values of $\Delta\sigma_P$ for prestrains greater than 1%.

Whilst experimental values of $\Delta\sigma_p$ for Q2N are shown as increasing linearly with prestrain (Equ 4.7), Figure 29a, they can be better characterised by fitting a compound curve similar to that associated with interfacial breakdown, Figure 29c, which can be described by the following equations:

$$\Delta\sigma_p^{Q2N} = 39.9(\pm 2.3) \times \epsilon_p \quad \ldots\ldots 5.1$$

Units: $\Delta\sigma$ [M Pa] : ϵ_p [%] : Equation determined by linear regression

Range: ϵ_p 0.25% → 1%

$$\Delta\sigma_p^{Q2N} = 21.5(\pm 0.4) \times \epsilon_p + 16.2(\pm 2.4) \quad \ldots\ldots 5.2$$

Units: $\Delta\sigma$ [M Pa] : ϵ_p [%] : Equation determined by linear regression

Range: ϵ_p 1% → 7.85%

Consequently, if the PEM/ABS model is to be applied to Q2N, in addition to determining accurate values for the variables in Equ 2.10, it will need to be modified to be able to accommodate particle / matrix interfacial breakdown.

5.5 Unified curve

From Figures 30 & 31 it can be seen that the BE exhibited by Q2N cannot be represented by a single *unified* reverse stress/strain curve. Whilst such a curve would have been extremely useful for theoretical submarine design calculations, the failure of the unified approach to characterise the BE exhibited by Q2N was not unexpected as it was principally developed to model the behaviour of single phase materials. The theory assumes that mobile dislocations interact during forward deformation to form a 3 dimensional cell structure with high dislocation density cell walls acting as localised regions with a high resistance to dislocation glide. Whilst these regions may be analogous to the elastic component of the PEM, implying that the unified approach might be

applicable to Q2N, the tenuous nature of this assertion is reflected by the inability of the unified approach to uniquely characterise Q2N. Furthermore, the success of the PEM, which takes no account of dislocation interaction mechanisms, may be indicative of their relative unimportance in describing the BE in two phase materials.

CHAPTER 6

FURTHER WORK

6.1 Introduction

With a few notable exceptions [33-36], the importance of the BE and the significant impact it can have on the integrity of a wide range of structural components, has yet to be fully appreciated by the wider engineering community. This may be due in part to the absence of an internationally recognised specification for measuring the BE, which in turn may be related to the somewhat uncoordinated approach towards the subject contained within the literature, and to the lack of a major structural failure directly attributed to the BE.

Therefore, if the BE is to gain greater acceptance and become a more important consideration in engineering design and fabrication processes, not only will an appropriate standard relating specifically to the BE have to be developed, it will also be necessary to characterise the effect in a broader range of structural materials. In addition, improvement of existing theoretical models for the BE and ways of reducing its magnitude will need to be addressed. These aspects of further work are now considered in more detail.

6.2 New applications / other materials

Although this present work has concentrated on the BE in Q2N as a candidate steel which may be used in the construction of future submarines for the Royal Navy, the material currently used for this application is Q1N. This steel has a similar composition and microstructure to Q2N, but has a lower tensile yield strength which is permitted to range from 550 MPa up to 690 MPa. Although the BE in Q1N has not been fully characterised, it is anticipated that its magnitude will be similar to that exhibited by Q2N, although this needs to be confirmed, and may be responsible for a reduction of about 20% in the ultimate bending strength of a submarine pressure hull fabricated from Q1N[13]. One consequence of this, is that such structures may be over designed

to compensate for this loss in strength. If it were possible to reduce or even remove altogether the influence of the BE, by heat treatment for example, this would then allow many components to be designed more efficiently and by implication, more cost effectively. In relation to the design and fabrication of submarines for the Royal Navy such cost savings could be in excess of £1,000,000 per boat.

The same argument is equally applicable to any structure, military or civilian, which has been designed without reference to the BE, examples of which might include oil rigs, bridges, commercial aircraft, pipelines, reactor vessels, ships, girders, etc. Unfortunately, because of a lack of information concerning the BE exhibited by the materials used in these applications, estimating potential cost savings is extremely difficult and would require further, more detailed investigation of the BE in each case.

It should also be noted, that inspite of the fact that welding has been universally adopted as one of the principal joining techniques, the literature did not contain a single reference to the BE in weld metals. Whilst the reason for this oversight is not immediately apparent, it is clear that this issue should be addressed sooner rather than later.

6.3 Reducing the BE

Having established that the BE in Q2N can cause a reduction in reverse yield strength of up to 50%, an obvious extention of the present work would be to consider ways in which its magnitude might be reduced. The effects of heat treatment have been briefly explored here, and have demonstrated that even a low temperature, short duration heat treatment (200°C for 30 minutes) after prestraining was able to bring about a 15% - 25% reduction in the BE. However, this finding is based on very limited testing and a more comprehensive program of work would be required to determine the influence of heat treatment and other relaxation mechanisms on the BE more accurately.

6.4 Improved modelling

Whilst a combination of the parallel elements model (PEM) and the Atkinson, Brown & Stobbs (ABS) model has been relatively successfully in characterising the BE exhibited by Q2N, its agreement with experimental observations is currently impaired by a lack precise data for some of the variables involved. In addition, the PEM/ABS model does not consider the size and distribution of hard second phase particles, and fails to take into account matrix/particle interfacial breakdown which is associated with prestrains in excess of 1%. Therefore, if the PEM/ABS model is to be integrated into the finite elements programs used by the Defence Research Agency in the design of ships and submarines for the Royal Navy, as is ultimately intended, further detailed theoretical work will be required to incorporate each of these factors.

CHAPTER 7

CONCLUSIONS

7.1 Characterising the Bauschinger effect

Several stress, strain and energy related parameters have been identified which may be used to evaluate the BE (listed below), which can be sub-divided into two groups refered to as *primary* and *secondary* BE parameters.

Stress related parameters	Strain related parameters	Energy related parameters
Primary Bauschinger Parameters		
$\Delta\sigma$ - The Bauschinger stress. Range: $0 \rightarrow$	ϵ_1 - The Bauschinger strain. Range: $0 \rightarrow$	E_S - The Bauschinger energy. Range: $0 \rightarrow$
Secondary Bauschinger Parameters		
β_σ - The Bauschinger Stress Parameter. Range: $0 \rightarrow 2$	β_ϵ - The Bauschinger Strain Parameter. Range: $0 \rightarrow 2$	β_E - The Bauschinger Energy Parameter. Range: $0 \rightarrow 1$

The primary BE parameters each have a value of zero where no BE exists, and express its magnitude in terms of a *specific* quantity, whilst the secondary BE parameters are bounded by a lower and an *upper* limit, and therefore give a measure of the *relative* magnitude of the BE. The most frequently quoted parameters are those related to stress, but their accuracy is dependant upon the precise measurement of yield strength during reverse deformation. Because Q2N does not exhibit a reverse yield point, it is necessary to use its 0.2% compressive proof stress as a measure of reverse yield strength and as a consequence the stress related BE parameters tend to over estimated the magnitude of the BE. However, the strain and energy related BE parameters can be measured without reference to a reverse yield event, and can therefore be determined more accurately. It should be noted that if the BE exhibited by Q2N is to be fully characterised, it is **essential** to quantify it using **all** of the stress, strain and energy related BE parameters, both *primary* and *secondary*.

7.2 Primary and secondary Bauschinger effect parameters

Experimental investigation of Q2N, a high strength naval steel, has shown that all the primary BE parameters increased linearly with increasing prestrain. The stress related secondary BE parameter, β_σ , also increased linearly with prestrain, but the strain and energy related secondary BE parameters, β_ϵ and β_E , decreased exponentially with prestrain.

7.3 Theoretical modelling

Predictive models which describe the BE theoretically have been successfully applied to Q2N, although their precision is currently impaired by of a lack of accurate data for some of the variables involved. Nevertheless, both prediction and, more importantly, experiment have demonstrated that the BE in Q2N is substantial, resulting in a reduction in reverse yield strength of up to 50%. This may have important implications for the design and performance of large fabricated structures such as submarines.

7.4 Further work

This preliminary investigation has highlighted the need for a more extensive study of the BE. Further work will consider the BE in a wider range of engineering materials and will focus on ways of reducing its magnitude. In addition, further effort will be directed towards improved modelling of the BE in order to enhance agreement between theoretical predictions and experimental observations.

ANNEX A

AN EXAMPLE OF THE CALCULATION OF THE BAUSCHINGER EFFECT PARAMETERS ASSOCIATED WITH A TYPICAL TC TEST

Establishing basic test parameters (Figure A1)

Extension associated with tensile prestraining (x_P) = 0.51mm

Gauge length of extensometer (GL) = 10mm

Tensile prestrain (ϵ_P) = (x_P / GL) . 100%

ϵ_P = **5.1%** (Engineering strain)

Maximum tensile load associated with prestraining (L_F) = 100 x 10^3 N

Cross sectional area of specimen (A) = 123.17 x 10^{-6} m^2

Engineering tensile prestress (σ_F) = L_F / A

σ_F = **811.8 MPa** (Engineering stress)

Calculation of stress related BE parameters

0.2% compressive proof load (0.2%L_R) = -53.75 x 10^3 N

0.2% compressive proof stress (0.2%σ_R)= 0.2%L_R / A

0.2%σ_R = -436.4MPa (Engineering stress)

Bauschinger stress ($\Delta\sigma$) = σ_F + 0.2%σ_R

$\Delta\sigma$ = **375.4MPa** (Engineering stress)

Bauchinger stress parameter (β_o) = $\Delta\sigma$/ σ_F

β_o = **0.462**

Permanent softening = $\Delta\sigma_P$

$\Delta\sigma_P$ = **125MPa** (True stress, Figure A2)

Calculation of strain related BE parameters

Reverse extension associated with full stress reversal (X_1) = 0.46 mm

Bauschinger strain (ϵ_1) = (X_1 / GL) . 100%

ϵ_1 = **4. 6%** (Engineering strain)

Bauschinger strain parameter (β_ϵ) = ϵ_1 / ϵ_P

β_ϵ = **0.901**

Calculation of energy related BE parameters

Work done (W) = Load (L) x extension (X) [units : joules (J)]

Each 1 mm^2 of Figure A1 is associated with an incremental load of 1250 N and an incremental extension of 0.005 mm. Consequently, each 1 mm^2 is connected with an amount of work equal to 6.25 mJ.

Area OABCO = 7710 mm^2

Prestrain work (W_P) = 7710 x 6.25 mJ

Hence $E_P = W_P / V = 39.2\ MJ/m^3$ Volume of specimen (V) = 1.23 x 10^{-6} m^3

Area CDEC = 1135 mm^2

Bauschinger work (W_S) = 1135 x 6.25 mJ

Hence $E_S = W_S / V = 5.77\ MJ/m^3$

Bauschinger energy parameter (β_E) = E_S / E_P

β_E = **0.147**

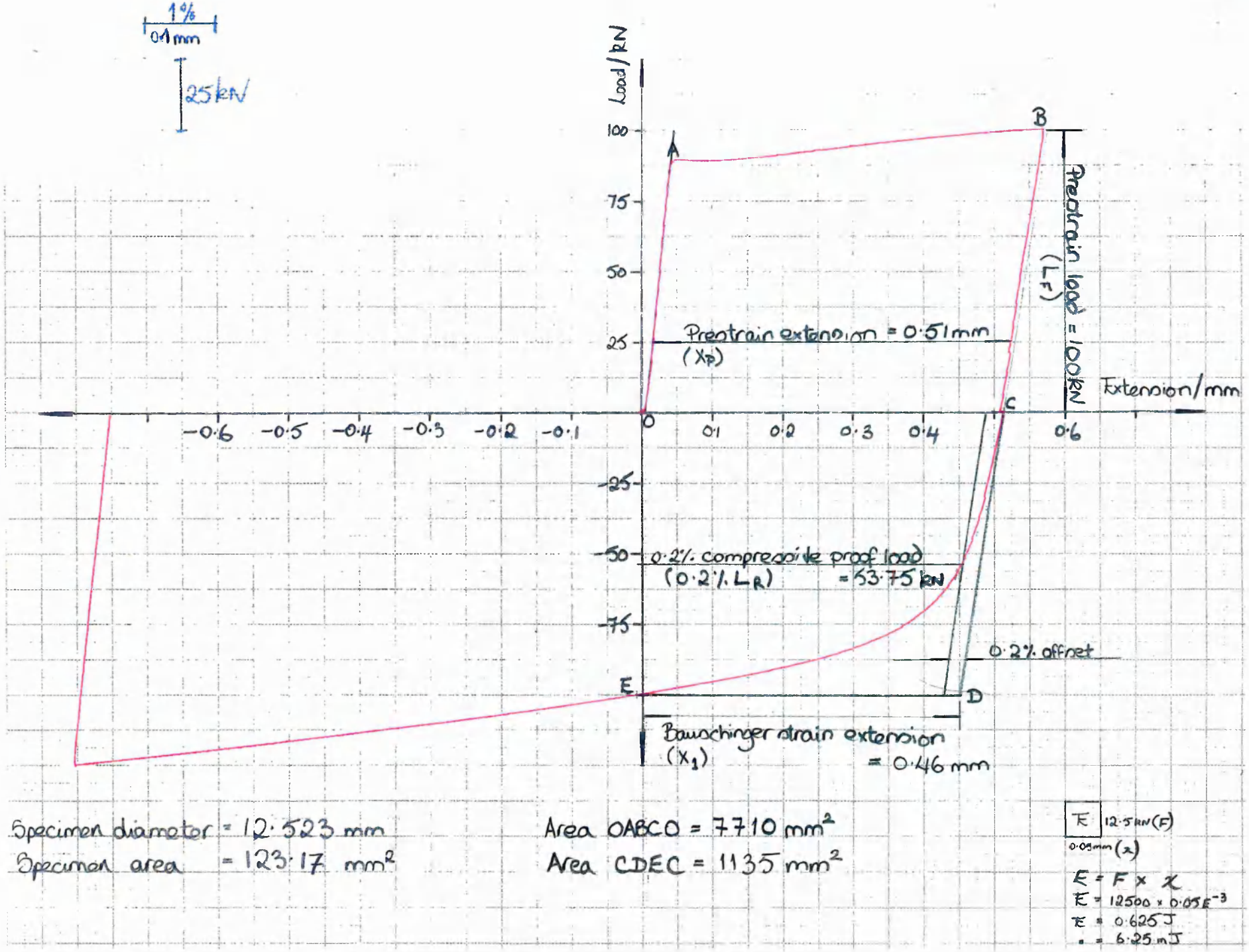
1%
0·1mm
25kN
Load/kN
100
75
50
25
-25
-50
-75
A
B
C
D
E
O
Pretrain load = 100kN (LF)
Pretrain extension = 0·51mm
(XP)
Extension/mm
-0·6
-0·5
-0·4
-0·3
-0·2
-0·1
0·1
0·2
0·3
0·4
0·6
0·2% compressive proof load
(0·2% LR) = 53·75 kN
0·2% offset
Bauschinger strain extension
(X1) = 0·46 mm
Specimen diameter = 12·523 mm
Specimen area = 123·17 mm²
Area OABCO = 7710 mm²
Area CDEC = 1135 mm²
E 12·5kN(F)
0·05mm(x)
E = F x x
E = 12500 x 0·05E⁻³
E = 0·625 J
= 6·25 mJ

Figure A1

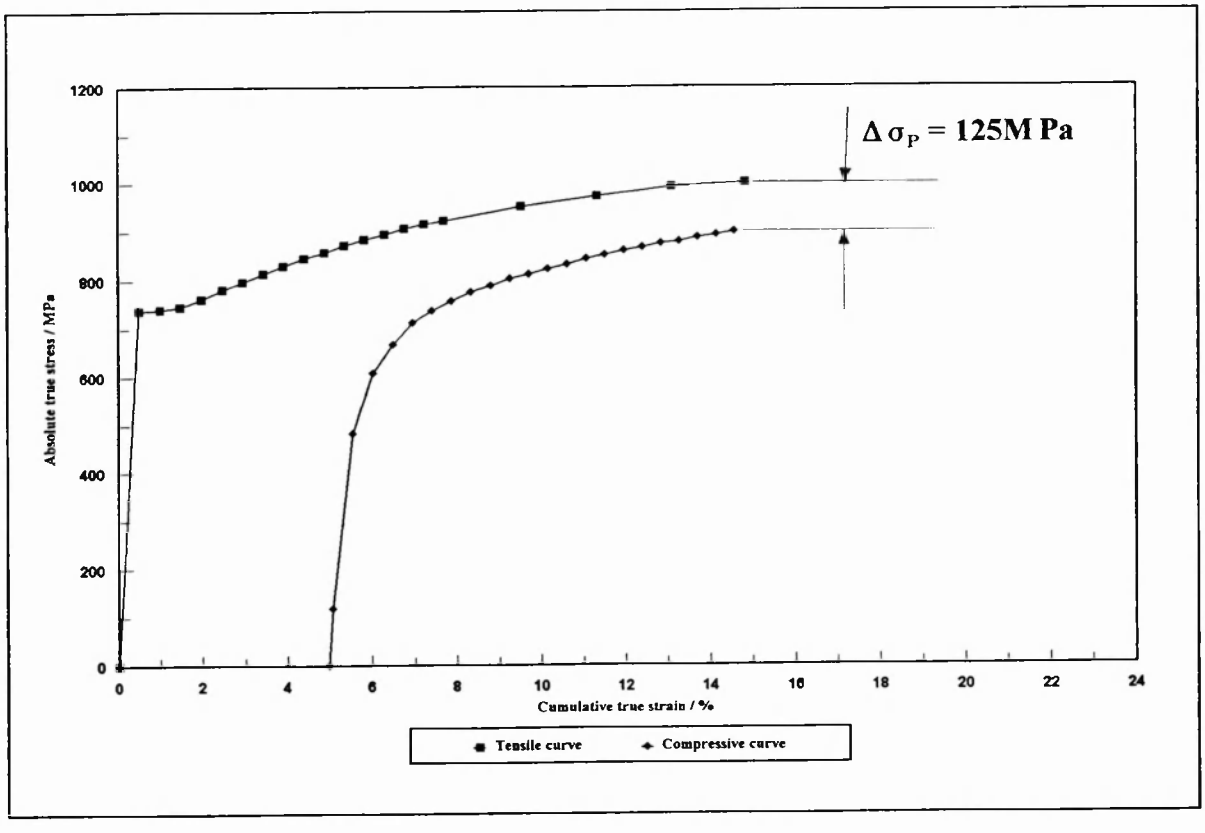

Measurement of the permanent softening, $\Delta\sigma_P$, exhibited

by Q2N after a tensile prestrain of 5.1%.

Figure A2

REFERENCES

1 BAUSCHINGER J., "Ueber die Veranderung der Elasticitatsgrenze und des Elasticitatsmoduls verschiedener Metalle.", Zivilingenieur, Vol. 27, col. 289 - 348, 1881.

2 ATKINSON J.D., BROWN L.M. & STOBBS W.M., "The Work Hardening of Copper-Silica IV. The Bauschinger Effect and Plastic Relaxation.", Philos. Mag., No.30, pp1247 - 1286, 1974.

3 TAYA M., LULAY K.E., WAKASHIMA K. & LLOYD D.J., "Bauschinger Effect in Particulate SiC - 6061 Aluminium Composites.", Materials Science and Engineering, A124, pp103 - 111, 1990.

4 TADASHI T., YAKOU T. & KOCKS U.F., "A Unified Representation of Stress-Strain Curves in Reversed Direction of Prestrained Cell-Forming Metals.", Transactions of the Japan Institute of Metals, Vol.27, No.6, pp425 -433, 1986.

5 ANGLADA M. & GUIU F., "The Bauschinger Effect in Cyclically Deformed Niobium Single Crystals.", Journal of Materials Science, 23, pp353 - 358, 1988.

6 YAMAN Y.M., AZSOY A. & TASCI K., "An Analysis of Bauschinger Parameters in Torsion.", Journal of Materials Science Letters, 9, pp429 - 431, 1990.

7 WOOLEY R.L., "The Bauschinger Effect in some Face Centred and Body Centred Cubic Metals.", Philos. Mag., No.44, pp597, 1953.

8 MacEWEN S.R., ELLS C.E & WOO O.T., "The Bauschinger Effect in Zircalloy-2.", Journal of Nuclear Materials, No.101, pp336 - 349, 1981.

9 LAY P. & BIRD J., "The Effect of Prestrain on the Tensile and Compressive 0.2% Proof Stress of Q2(N) Steel. (Unclassified)", ARE TM (USE) 88209, Admiralty Research Establishment, Procurement Executive, Ministry of Defense, Dunfermline, Fife, Scotland, November 1988.

10 Naval Engineering Standard 826, "Requirements for Q2(Navy) Quality Steel, Part 1 - Issue 1 (Plate).", Procurement Executive, Ministry of Defense, Deputy Controller Warship Equipment, Foxhill, Bath, United Kingdom, November 1986.

11 BROWN P. M. & McGOWAN C. D., "The Effect of Stress Relief on the Mechanical Properties of Q2N.", Defence Research Agency, SMC Scotland, Farnborough, Hampshire, England, GU14 6TD, 1995, To be published.

12 BROWN P. M., "The Effect of various Heat Treatments on the Tensile Properties of Q2(N) Steel. (Unclassified)", ARE TM (UHS) 90216, Admiralty Research Establishment, Procurement Executive, Ministry of Defense, Dunfermline, Fife, Scotland, May 1990.

13 MITCHELL G. C., BROWN P. M. & WILSON P., "A Review of the Bauschinger Effect in relation to the Strength of Submarine Pressure Hulls. (Unclassified)", DRA/AW/AWS/CR94267, Defence Research Agency, Farnborough, Hampshire, England, GU14 6TD.

14 GOULD D., HIRSCH P.B. & HUMPHREYS F.J., "The Bauschinger Effect, Work Hardening and Recovery in Dispersion Hardened Copper Crystals.", Philos. Mag., No.30, pp1353 - 1377, 1974.

15 WANG Z. & MARGOLIN H., "The Interaction of Surface and Interior to produce Bauschinger Behaviour in 70 - 30 Alpha-Brass Single Crystals Oriented for Easy Glide.", Res. Mechanica, 21, pp249 - 286, 1987.

16 STOBBS W.M. & PAETKE S., "The Bauschinger Effect in Cold Drawn Patented Wire.", Acta Metallurgica, Vol.33, No.5, pp777 - 783, 1985.

17 ARSENAULT R.J. & WU S.B., "The Strength Differential and Bauschinger Effect in SiC-Al Composites.", Materials Science and Engineering, Vol.96, pp77 - 88, 1987.

18 STOUT M.G., & ROLLET A.D., "Large Strain Bauschinger Effects in FCC Metals and Alloys.", Metallurgical Transactions A, Vol.21A, pp3201 - 3213, December 1990.

19 WILSON D.V., "Reversible Work Hardening in Alloys of Cubic Metals.", Acta Metallurgica, Vol.13, pp807 - 814, July 1965.

20 MIYAUCHI K., "Stress-Strain Relationship in Simple Shear of In-plane Deformation for various Steel Sheets.", Proc. 13th IDORG Congress, Melbourne, 1984.

21 WILSON D.V. & KONNAN Y.A., "Work Hardening in a Steel containing a Coarse Dispersion of Cementite Particles.", Acta Metallurgica, Vol.12, pp617 - 628, May 1964.

22 WILSON D.V. & BATE P., "Reversibility in the Work Hardening of Spheroidised Steels.", Acta Metallurgica, Vol.34, No.6, pp1107 - 1120, 1986.

23 EBENER H., "Acoustic Emission and the Bauschinger Effect in Cu Single Crystals.", Scripta Metallurgica, Vol.25, pp2035 - 2040, 1991.

24 ABEL A. & MUIR H., "The Bauschinger Effect and Discontinuous Yielding.", Philos. Mag., No.26, pp489 - 504, 1972.

25 WILSON D.V. & BATE P., "Indentification of the Mean Internal Stress from the Bauschinger Stress.", Scripta Metallurgica, Vol.20, pp1529 - 1533, 1986.

26 MASING G., Wissenschaftl. Veroffentl. a.d. Siemens-Konzern 3, pp231, 1923.

27 TENNENT R.,"Science Data Book.", Published by Oliver & Boyd, ISBN 0 05 002487 6, 1978.

28 Personal communication with Professor Terry Gladman, School of Materials, The University of Leeds.

29 Personal communication with Dr. Ron Stephens, School of Materials, The University of Leeds.

30 Procedure for Estimating Uncertainty of Measurement, Procedure No: MTL T04, Mechanical Testing Laboratory, Structural Materials Centre, Defence Research Agency, Dunfermline, Scotland, KY11 2XR.

31 TANAKA K., MORI T, & NAKAMURA T., "Cavity Formation at the Interface of a Spherical Inclusion in a Plastically Deformed Matrix.", Philos. Mag., No 21, pp267 - 279, 1970.

32 STOLTZ R.E. & PELLOUX R. M., "The Bauschinger Effect in Precipitation Strengthened Aluminium Alloys.", Metallurgical Transactions A, Vol.7A, pp1295 - 1306, September 1976.

33 STACEY A. & WEBSTER G. A., "Determination of Residual Stress Distributions in Autofrettaged Tubing.", International Journal of Pressure Vessels and Piping, Vol. 31, pp205 - 220, 1988.

34 YONG L. & NAIJIE S., "Residual Stresses Analysis for Actual Material Model of Autofrettaged Tube by Non-linear Boundary Element Method.", International Journal of Pressure Vessels and Piping, Vol. 48, pp21 - 35, 1991.

35 SCHMIDT L. C., LU J. P. & MORGAN P. R., "The Influence on Steel Tubular Strut Load Capacity of Strain Hardening, Strain Aging and the Bauschinger Effect.", J. Construct. Steel Research, Vol.14, pp107 - 119, 1989.

36 KANISAWA H. & MORI T., " Development of wire rod with low flow stress for non-heat treated fasteners.", 59th Annual Convention and 1989 Division Meetings, Atlanta, Georgia, pp178 - 183, published by Wire Association International, P.O Box H, 1570 Boston Post Road, Guilford, Connecticut 06437, USA, 1990.

Source / Element	C	Si	Mn	P	S	Cr	Mo	Ni	Al	As	Cu	N_2	Sn	V	Pb	Sb	O_2
Plate 7483	0.15	0.33	0.43	0.011	0.006	1.61	0.51	3.39	0.04	0.02	0.12	0.010	0.02	0.06	<0.001	<0.001	0.007
Min NES 826	0.11	0.15	0.30			1.30	0.40	3.15						0.05			
Max	0.16	0.35	0.50	0.015	0.015	1.80	0.60	3.65		0.03	0.20	0.015	0.02	0.10	0.0025	0.010	

Chemical Analysis of Q2N Plate 7483.

Table 1

Material	$\frac{(\Delta \sigma_p / \sigma_F)}{\%}$
Al - 3% Mg	15
Decarburised steel	14
Duralumin	44
1.1%C steel	42

Examples of the permanent softening exhibited by single and two phase materials

Table 2

ϵ_P / %	σ_F / MPa	$0.2\%\sigma_R$ / MPa	$\Delta\sigma^*$ / MPa	$\beta_\sigma{}^*$	ϵ_1 / %	β_ϵ	E_S / MJ/m^3	E_P / MJ/m^3	β_E	$\Delta\sigma_P$ / MPa
0.25	-	-	-	-	-	-	-	-	-	9
0.48	728	-464	264	0.36	0.82	1.70	1.2	3.7	0.33	-
0.60	-	-	-	-	-	-	-	-	-	27
0.92	729	-432	297	0.41	1.27	1.38	1.5	6.7	0.24	35
2.20	762	-388	374	0.49	2.47	1.12	3.1	16.5	0.19	70
3.05	782	-441	341	0.44	3.06	1.00	3.8	23.1	0.17	80
3.81	799	-446	353	0.44	3.52	0.92	4.4	29.4	0.15	100
5.10	812	-436	376	0.46	4.60	0.90	5.8	39.2	0.15	125
5.10$^+$	811	-491	320	0.39	3.95	0.77	4.3	39.2	0.11	100
5.85	826	-448	378	0.46	5.41	0.93	5.5	45.4	0.12	142
6.97	833	-407	426	0.51	6.00	0.86	6.2	53.2	0.12	170
7.85	831	-397	434	0.52	6.40	0.82	7.2	61.5	0.12	182
8.10	829	-398	431	0.52	6.40	0.79	5.9	61.1	0.10	-

* Calculated using the 0.2% compressive proof stress, $0.2\%\sigma_R$, as a measure of compressive yield strength.

+ Specimen heat treated at 200C for 30 mins after being prestrained.

Experimental Bauschinger Data for Q2N

Table 3

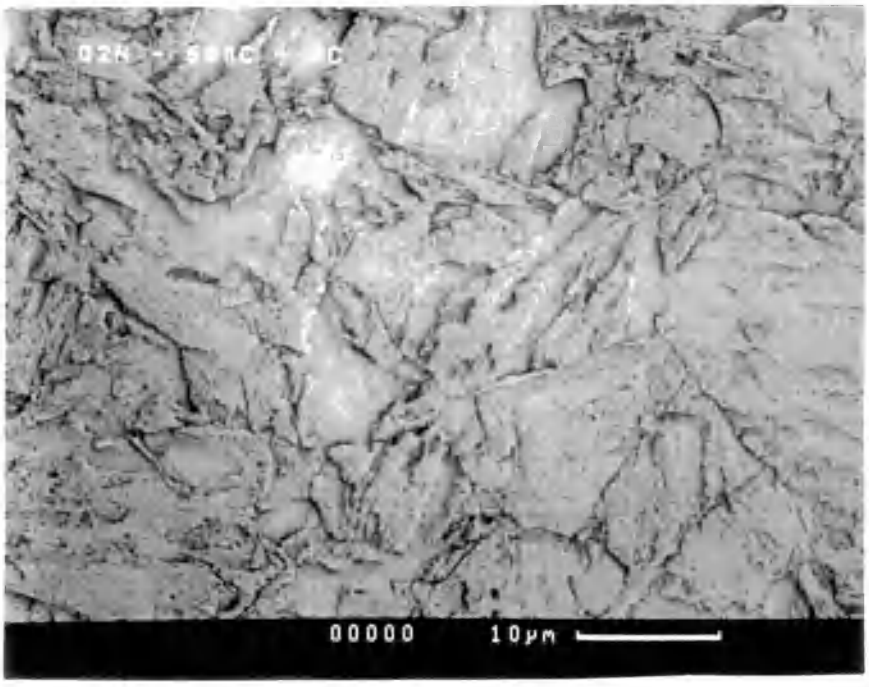

a) Scanning electron micrograph of Q2N showing a microstructure of tempered martensite containing a fine distribution of carbides.

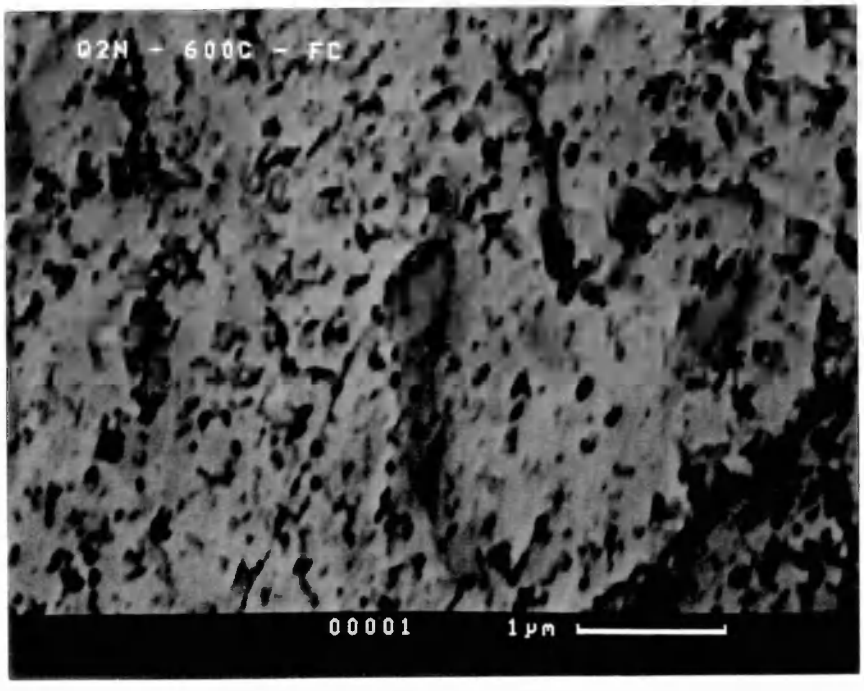

(b) Scanning electron micrograph of Q2N showing carbide distribution.

Figure 1

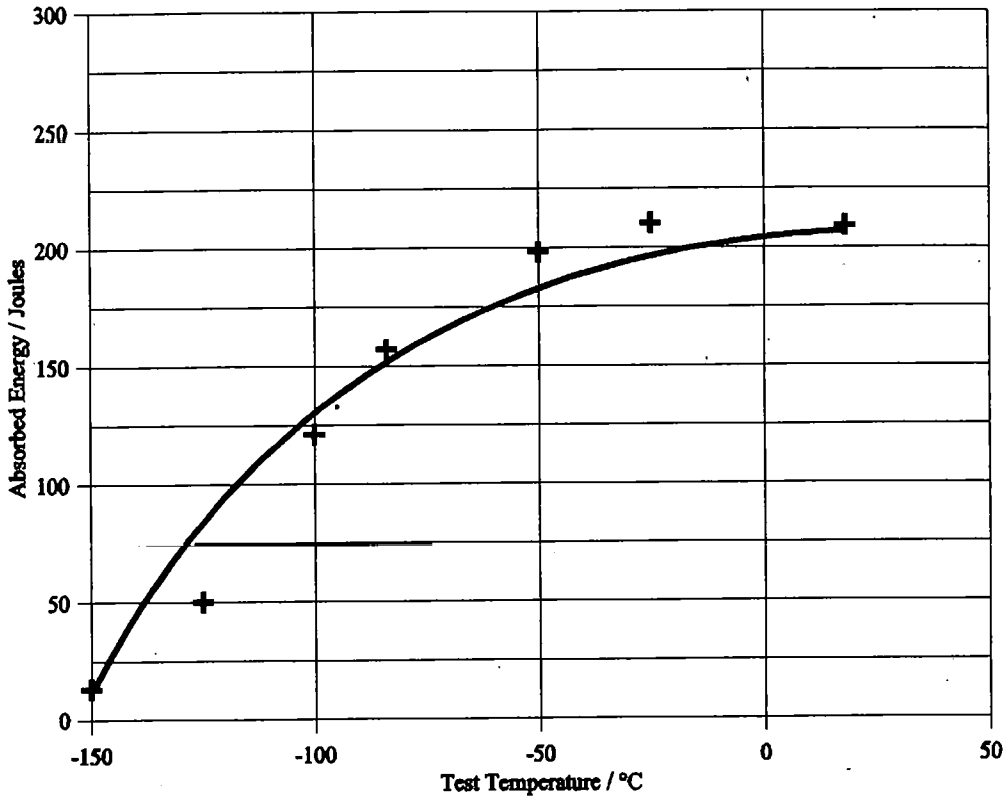

Charpy transition curve for Q2N in its quenched and tempered condition.

Figure 2

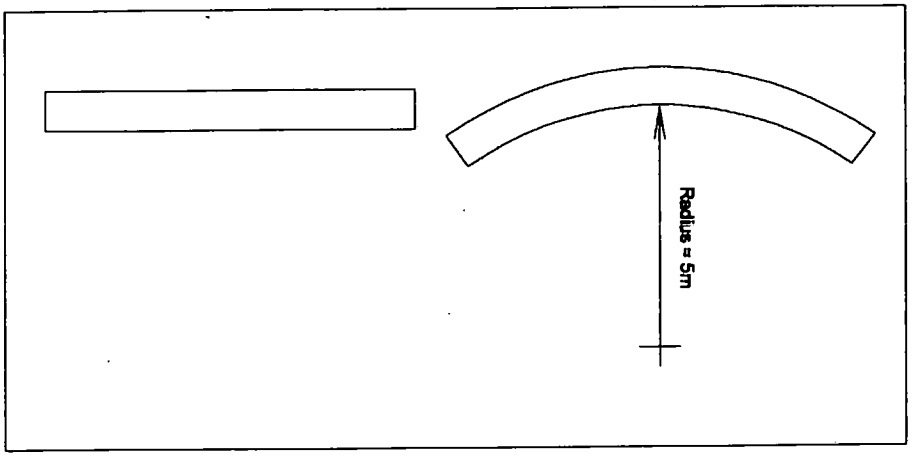

(a) Typical submarine pressure hull radius.

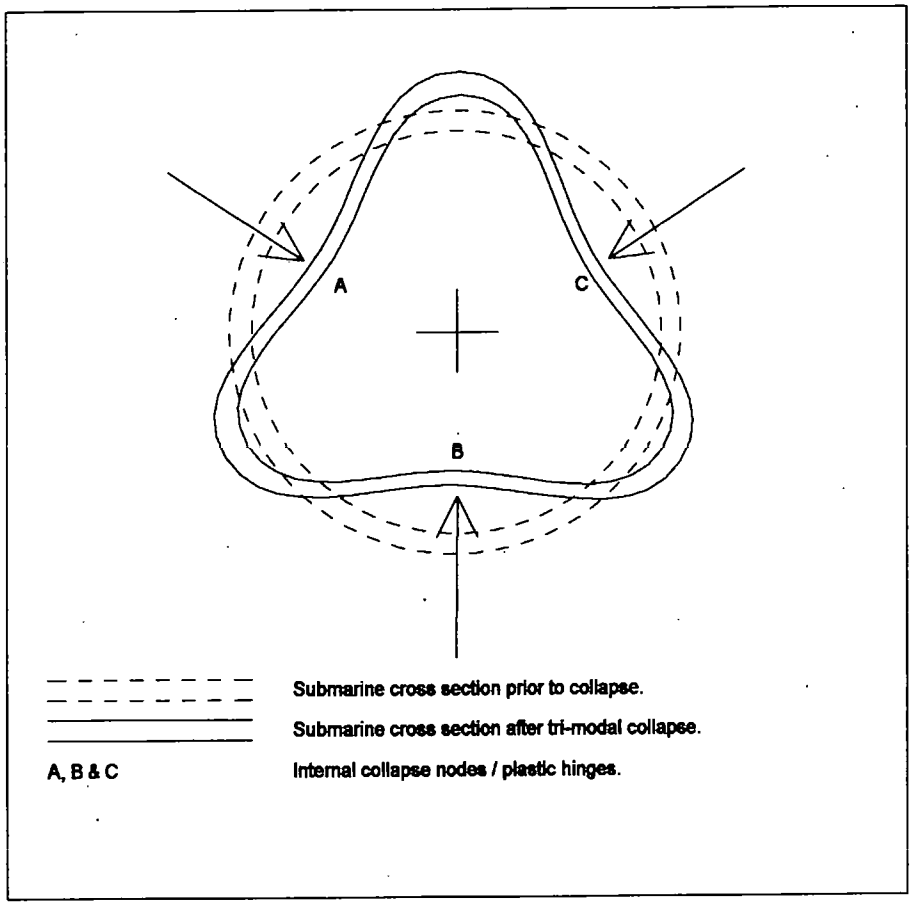

(b) Tri-modal submarine collapse at maximum dive depth.

Figure 3

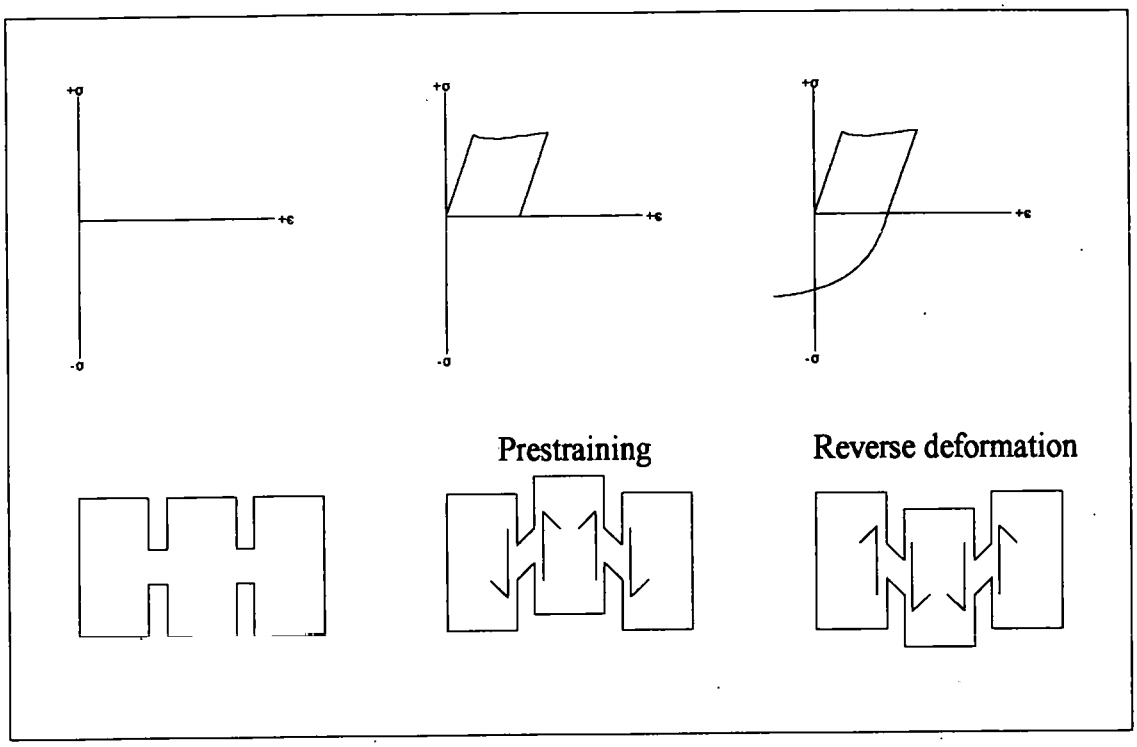

(a) A schematic representation of the planar simple shear (PSS) test.

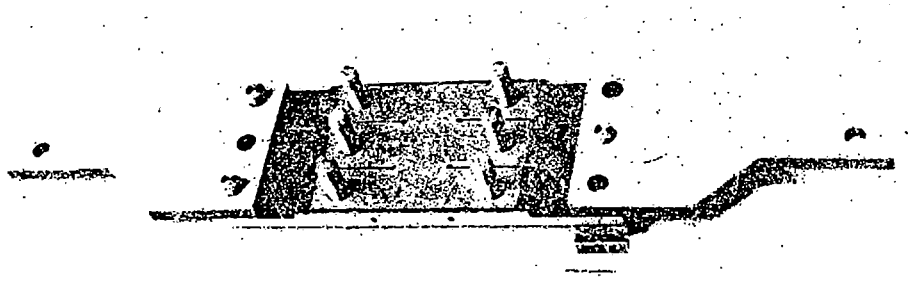

(b) Photograph of the PSS test specimen [20]

Figure 4

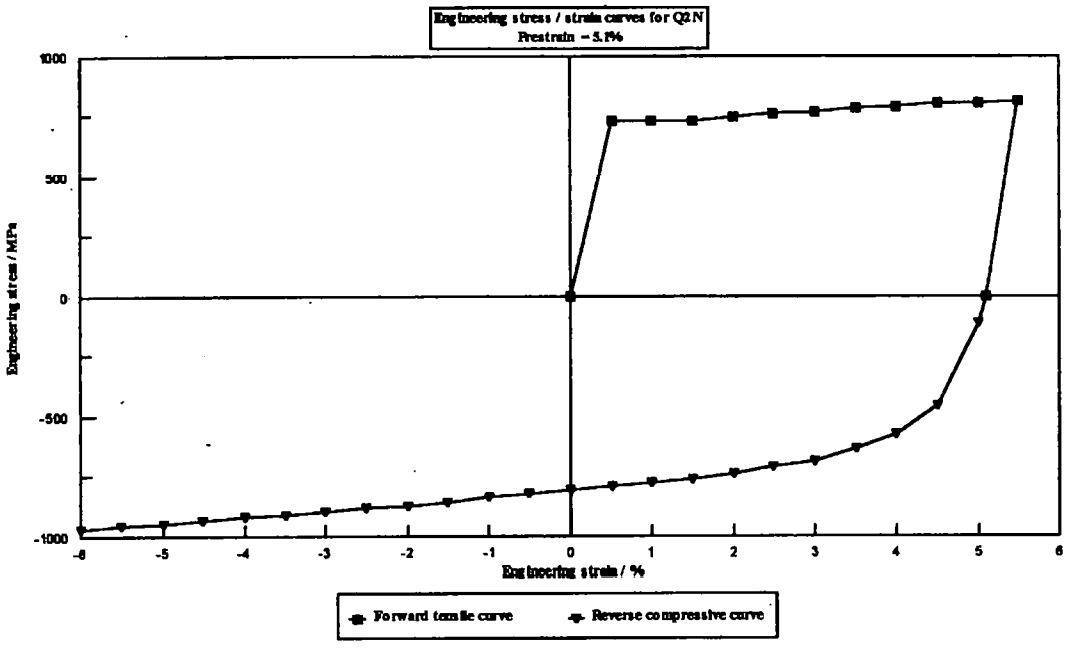

(a) Typical TC test engineering σ / ϵ curve.

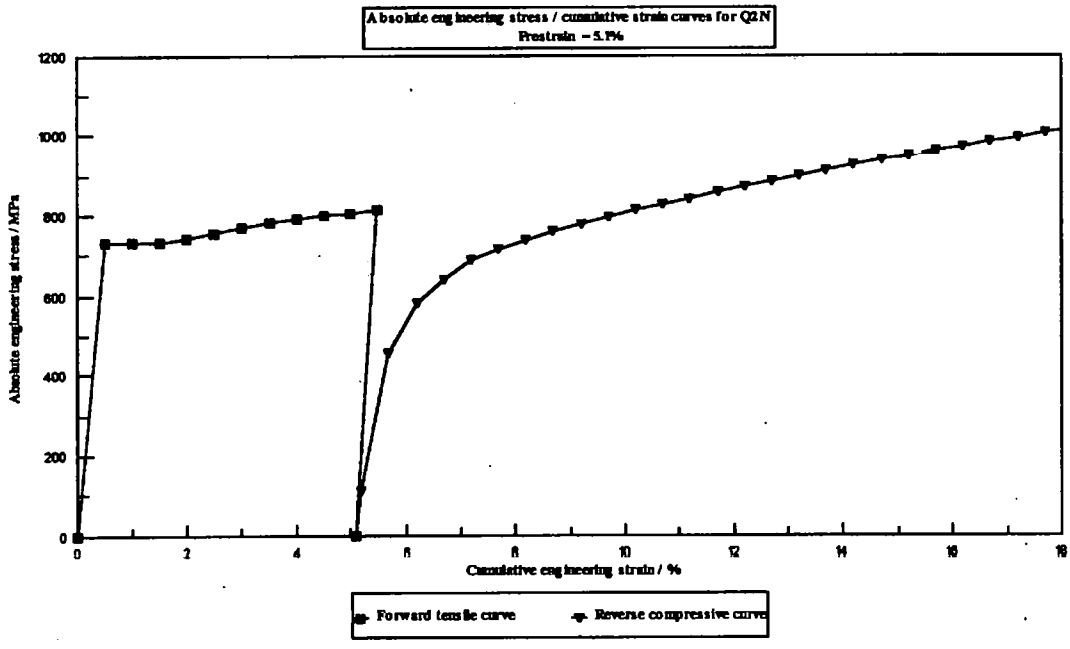

(b) Figure 5a plotted in terms of absolute stress and cumulative strain.

Figure 5

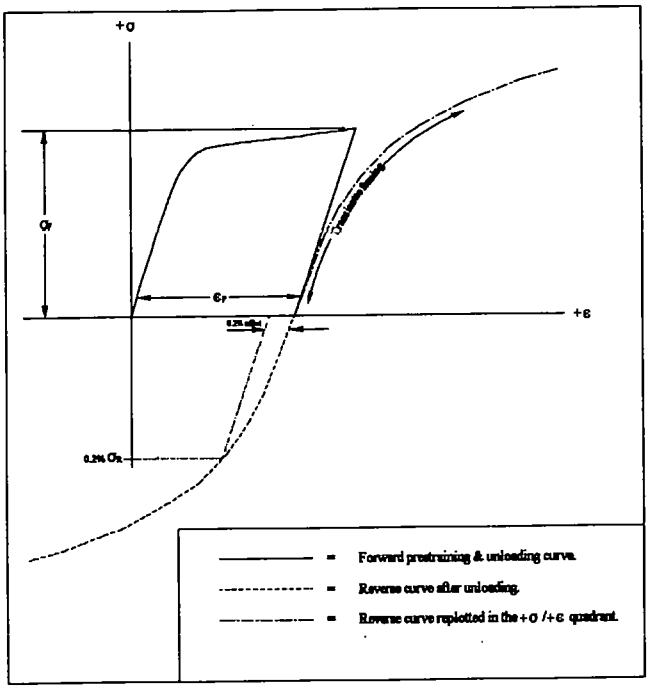

$$| 0.2\%\sigma_R | < | \sigma_F |$$

$\Delta\sigma$ = Bauschinger stress.

$$\Delta\sigma = 0.2\%\sigma_R + \sigma_F$$

$\Delta\sigma = 0$ where no Bauschinger effect exists.

β_σ = Bauschinger stress parameter.

$$\beta_\sigma = \Delta\sigma / \sigma_F$$

$$0 \leq \beta_\sigma \leq 2$$

A schematic representation of the stress related BE parameters determined from the engineering σ / ϵ curve of a typical TC test.

Figure 6a

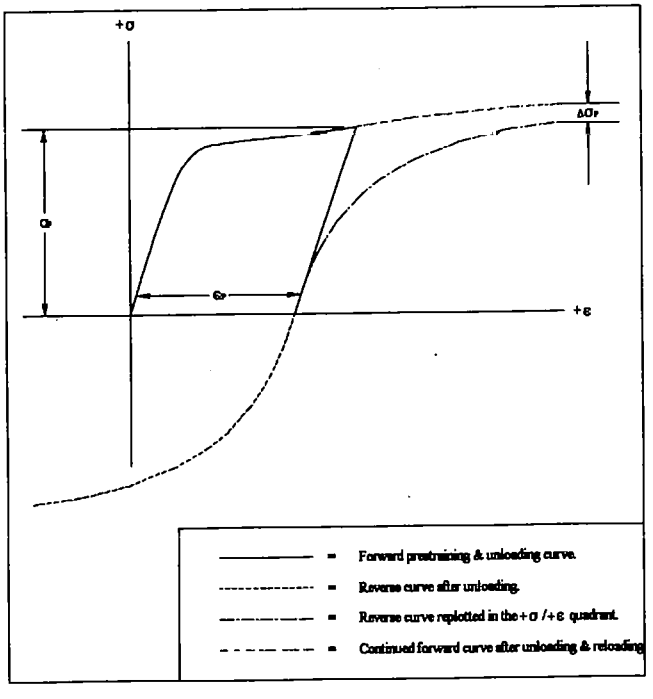

A schematic representation of permanent softening, $\Delta\sigma_P$, determined from the true σ / ϵ curve of a typical TC test.

Figure 6b

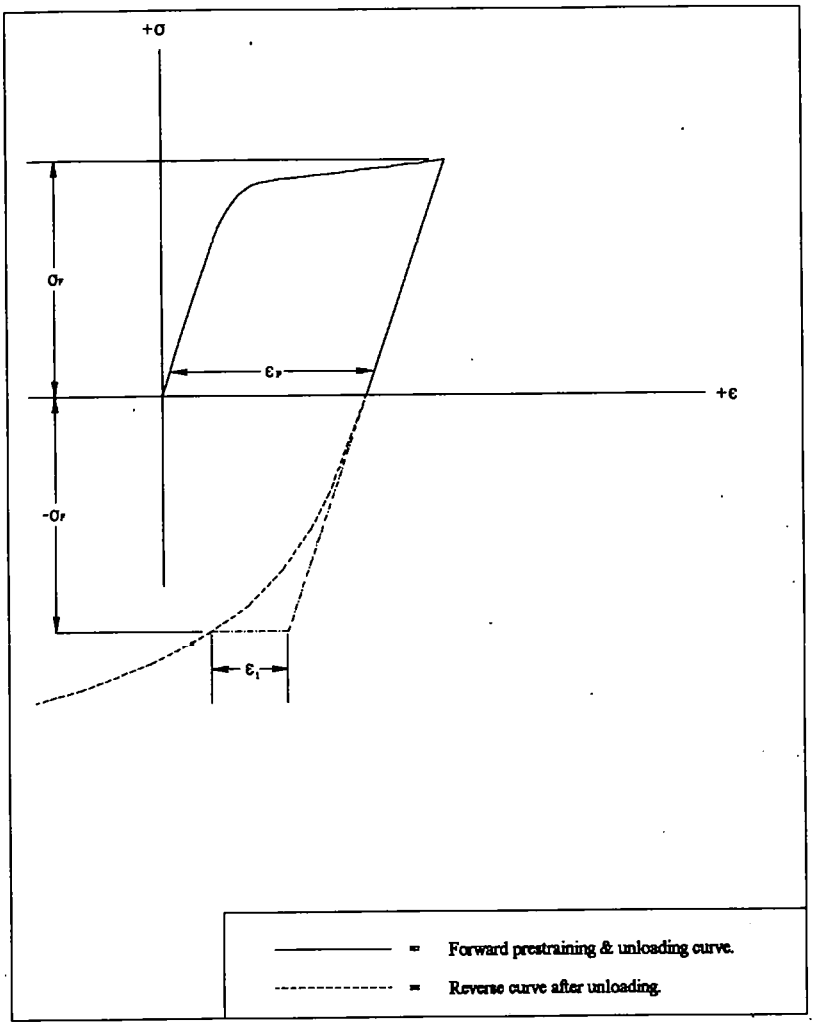

ϵ_1 = Bauschinger strain

$\epsilon_1 = 0$ where no BE exists

β_ϵ = Bauschinger strain parameter

$$\beta_\epsilon = \epsilon_1 / \epsilon_P$$

$$0 \leq \beta_\epsilon \leq 2$$

A schematic representation of the strain related BE parameters determined from the engineering σ / ϵ curve of a typical TC test.

Figure 7

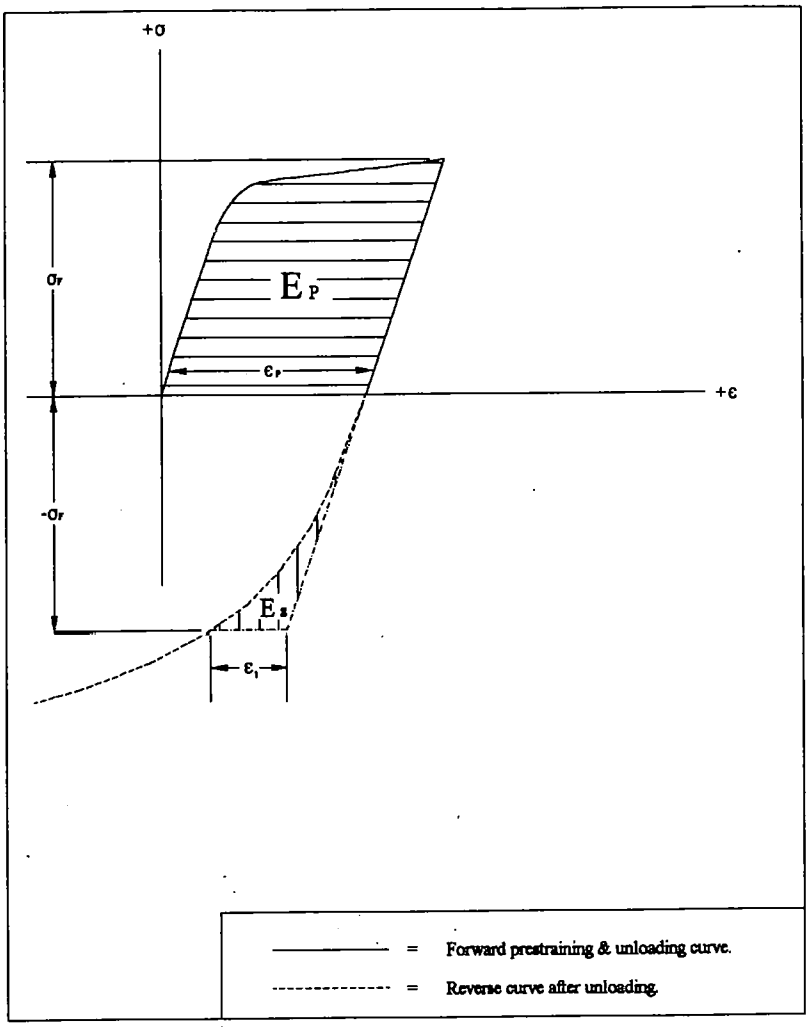

E_S = Bauschinger energy

E_P = Prestrain energy

$E_S = 0$ where no BE exists

β_E = Bauschinger energy parameter

$\beta_E = E_S / E_P$

$0 \leq \beta_E \leq 1$

A schematic representation of the energy related BE parameters determined from the engineering σ / ϵ curve of a typical TC test.

Figure 8

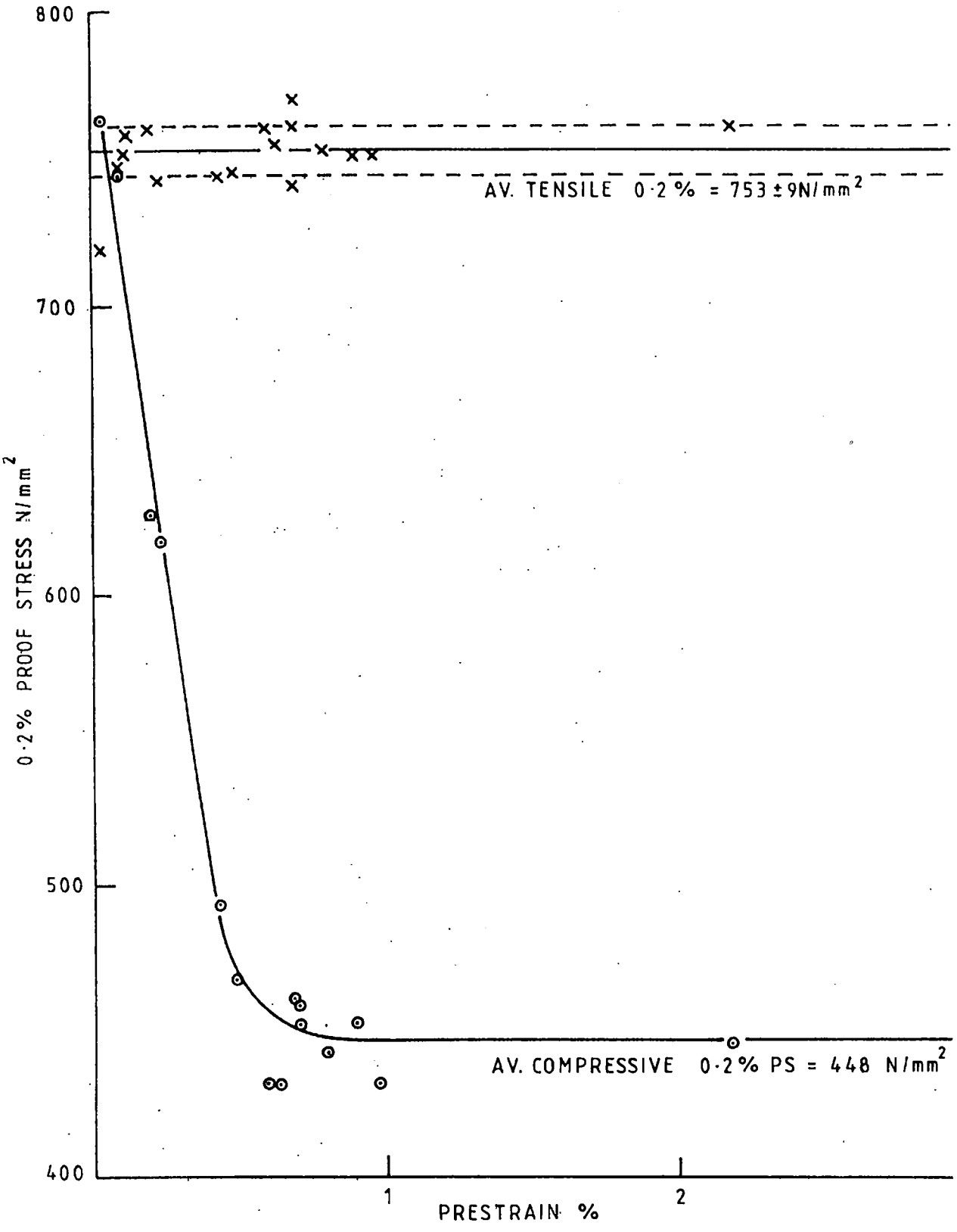

The effect of tensile prestrain on the 0.2% compressive proof stress of Q2N [9].

Figure 9

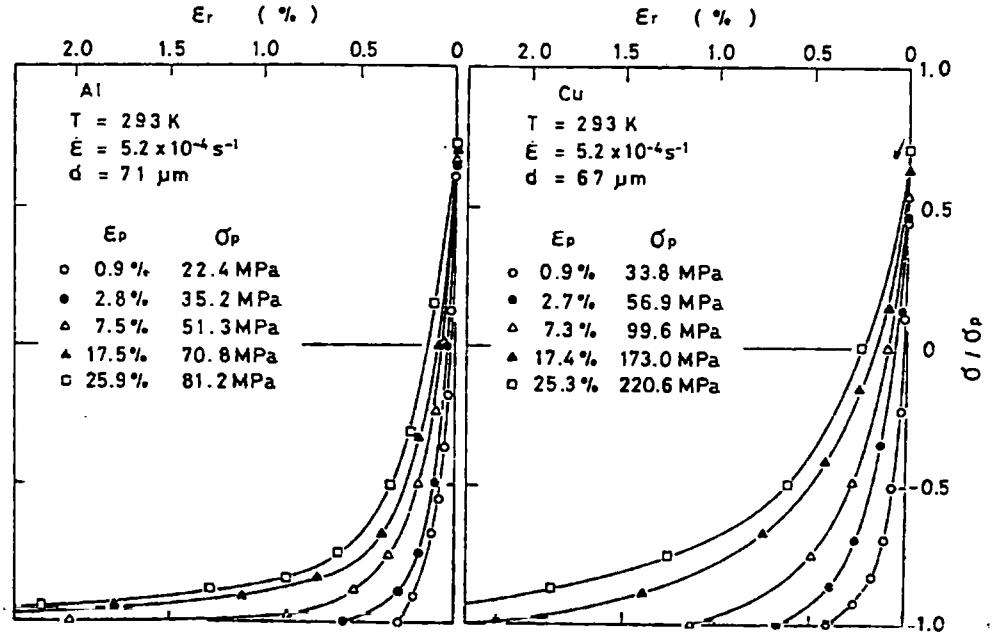

(a) Reverse true σ / ϵ curves for aluminium [4]

(b) Reverse true σ / ϵ curves for copper [4]

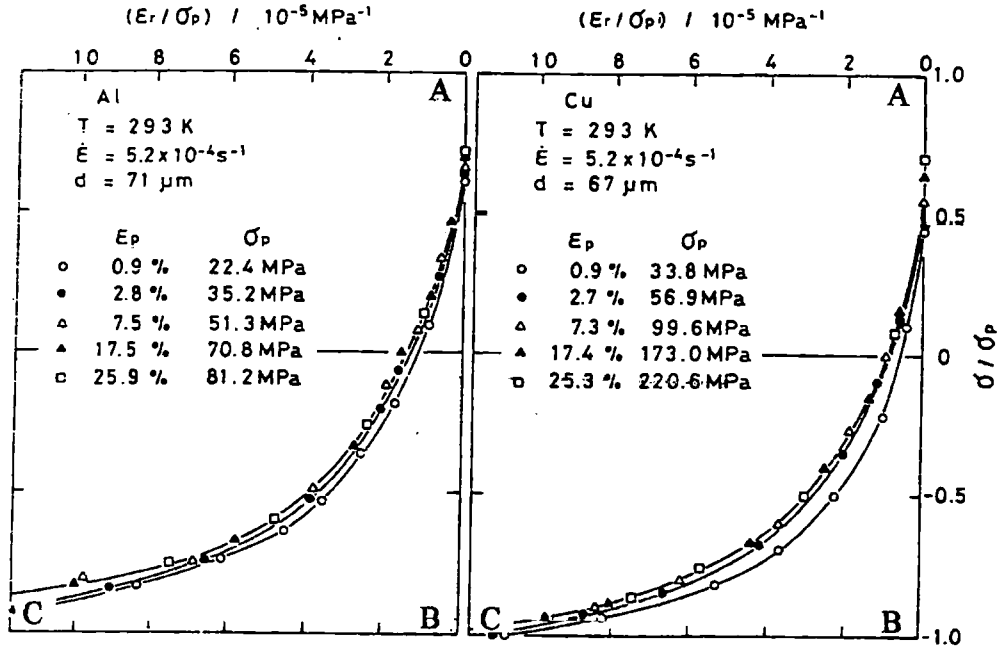

(c) Unified curves for aluminium[4]

(d) Unified curves for copper [4]

Figure 10

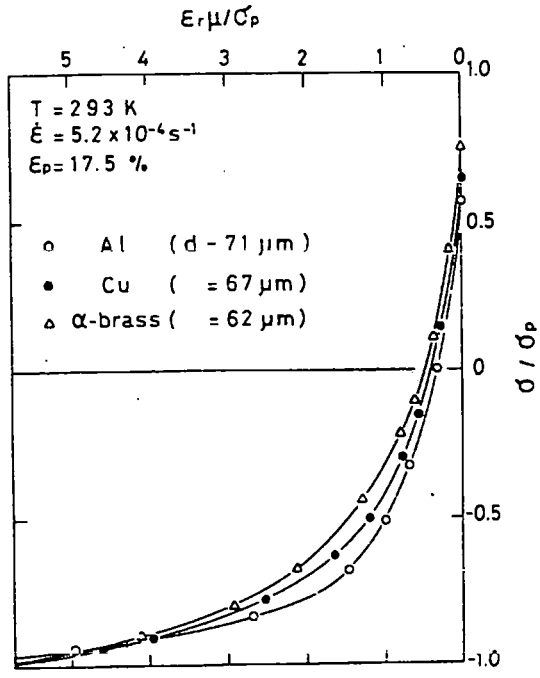

μ = shear modulus of each material at a temperature T.

Unified curves for aluminium, copper and α-brass [4]

Figure 11

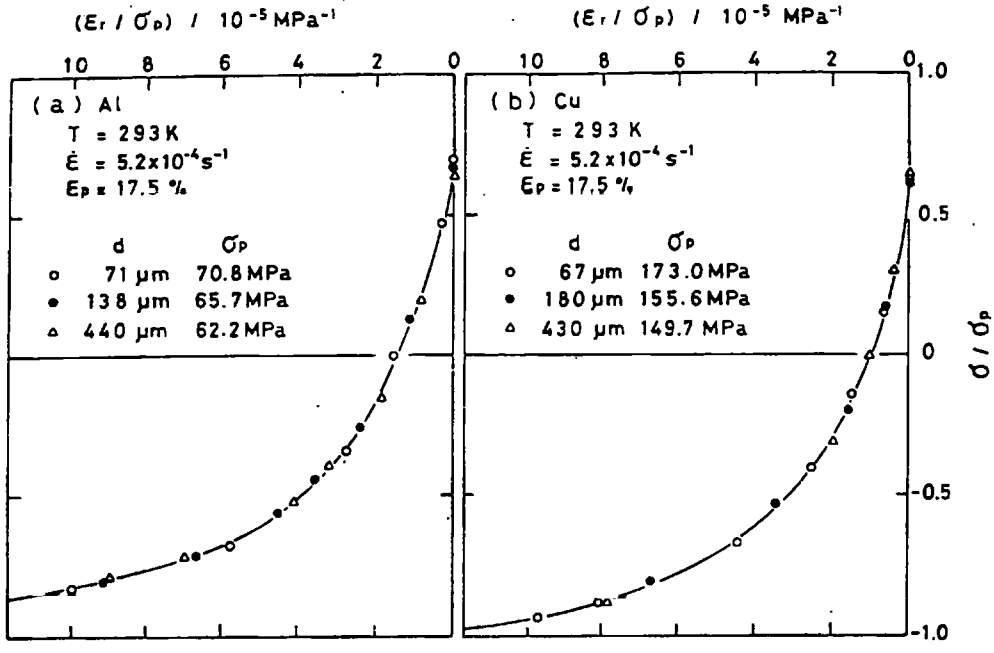

(a) The effect of grain size on the unified curve for aluminium[4]

(b) The effect of grain size on the unified curve for copper [4]

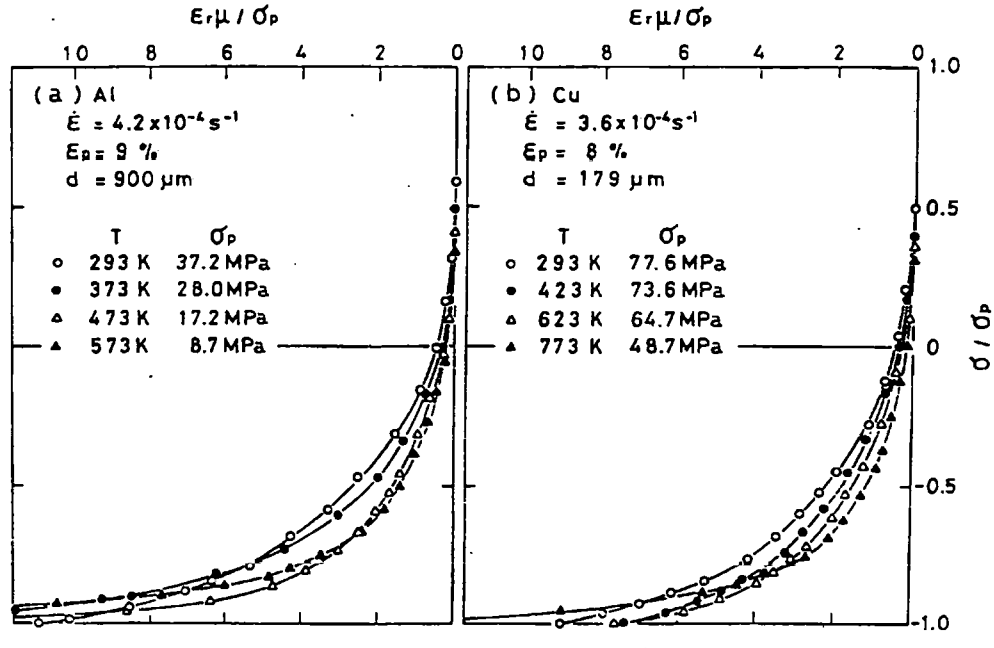

(c) The effect of temperature on the unified curve for aluminium [4]

(d) The effect of temperature on the unified curve for copper [4]

Figure 12

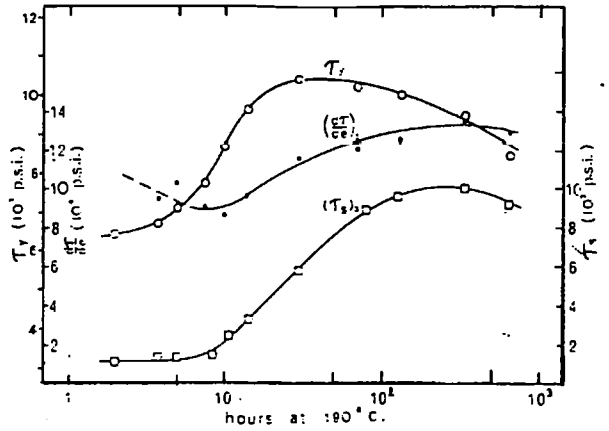

(a) The effect of ageing time on the shear yield strength (τ_Y) and permanent softening (τ_S) exhibited by Al - 4%Cu [19]

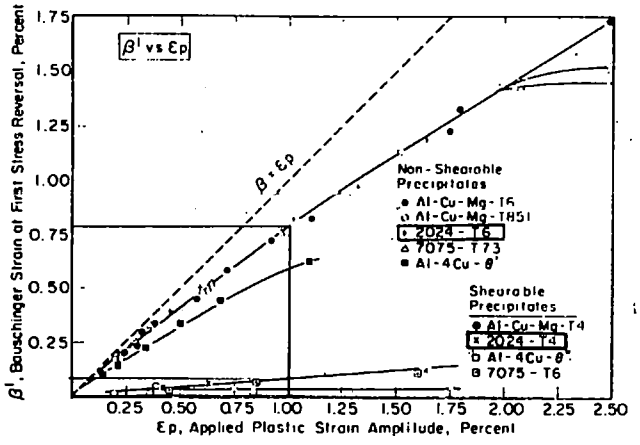

(b) The effect of prestrain on the Bauschinger strain (β_1) exhibited by materials containing shearable and non-shearable precipitates [32]

Figure 13

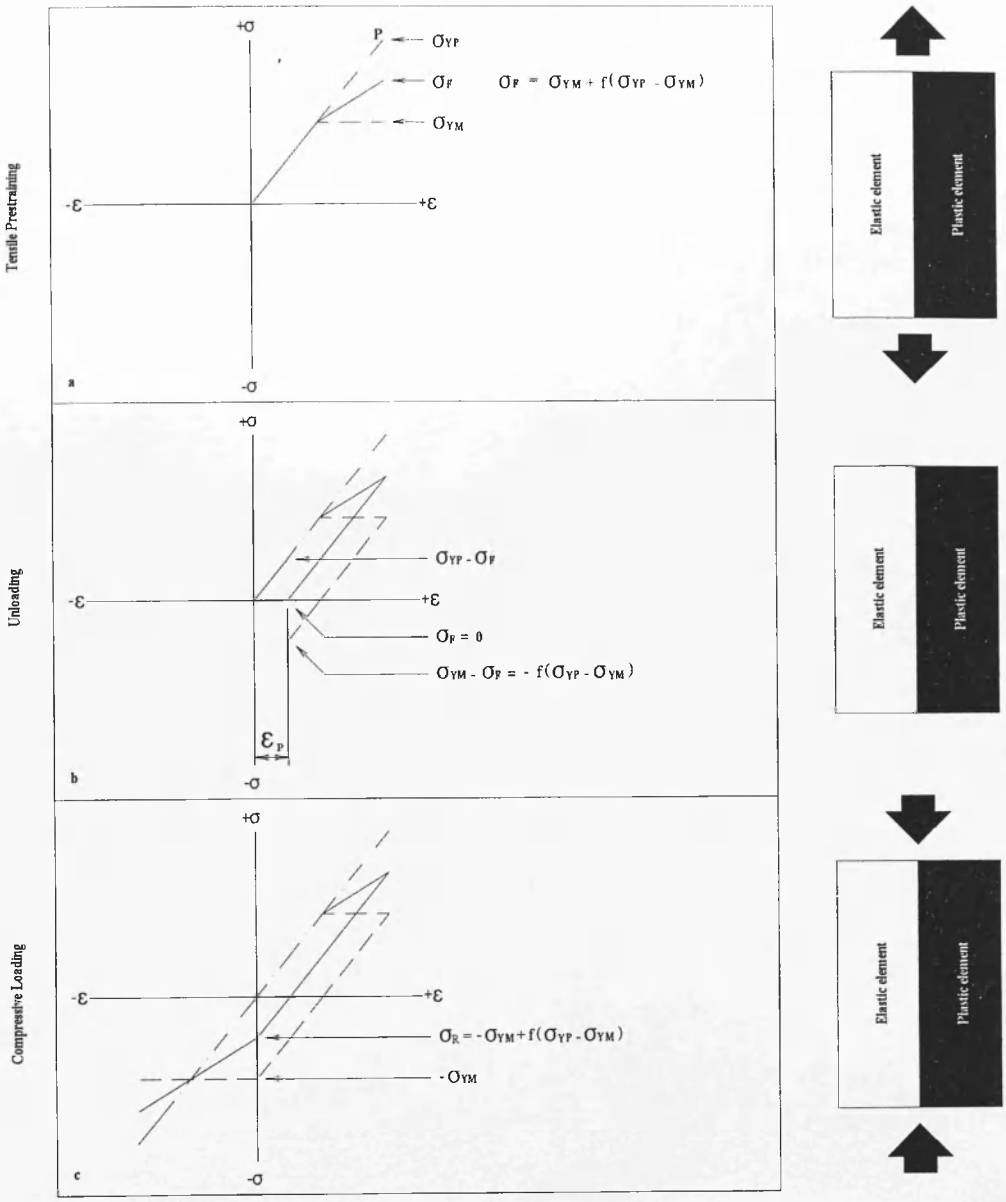

– – – – – – = Stress in elastic element / particle.

– – – – – – = Stress in plastic element / matrix.

———— = Composite stress / strain curve.

A schematic representation of the Parallel Elements Model (PEM), showing the stresses and strains experienced by the elastic and plastic elements of a composite specimen, during forward and reverse loading.

Figure 14

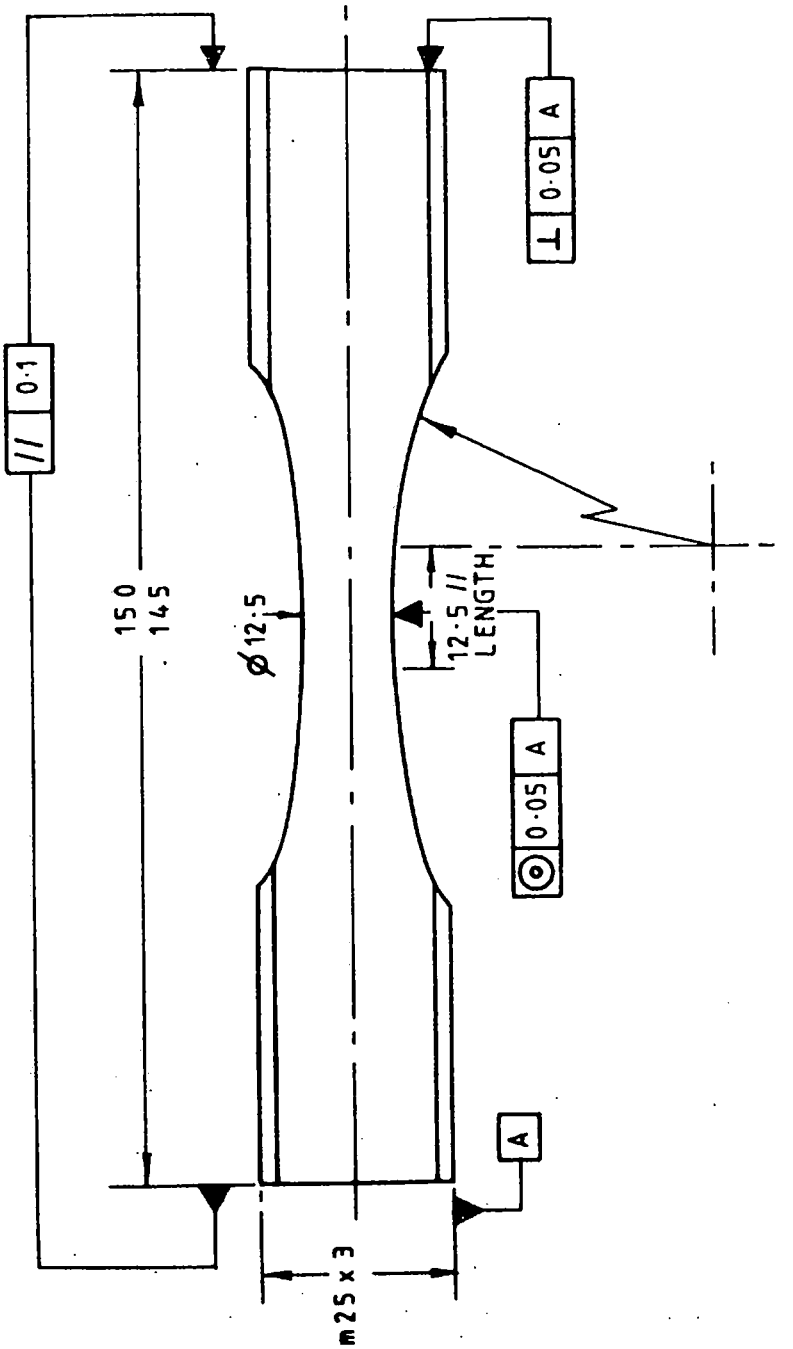

dimensions in mm

Diagram of a TC test specimen.

Figure 15

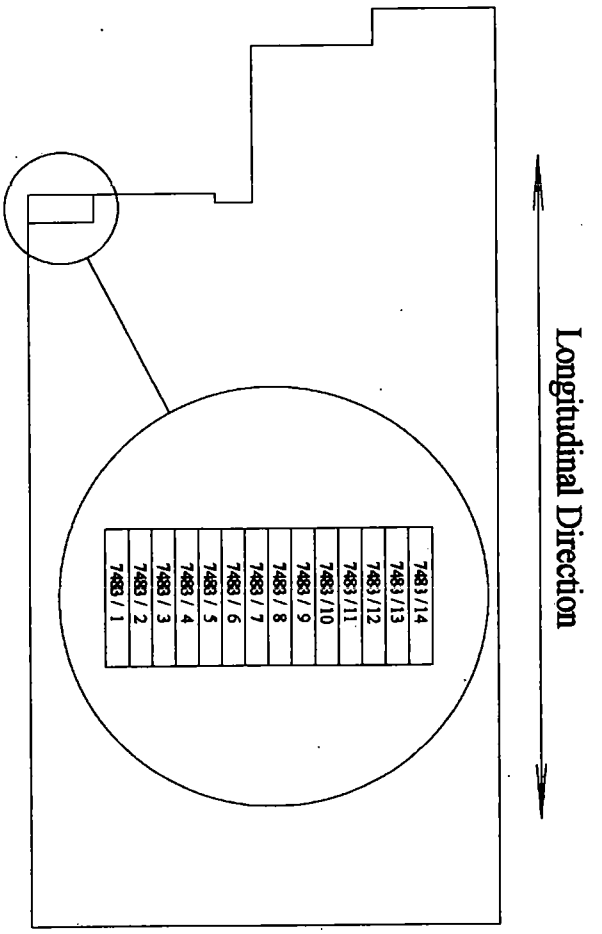

plate thickness = 25.4mm

Orientation of TC test specimens machined from Q2N plate 7483

Figure 16

250 kN ESH servo-hydraulic machine used for TC testing.

Figure 17

SANDNER 10 - 5X extensometer with a gauge length of 10mm, capable of measuring extensions of ±2mm to an accuracy of ±1μm.

Figure 18

TC specimen used for alignment check of 250 kN servo-hydralic testing machine (Fig. 17) with strain gauges at 90°, 180°, 270° and 360° positions around its gauge length.

Figure 19

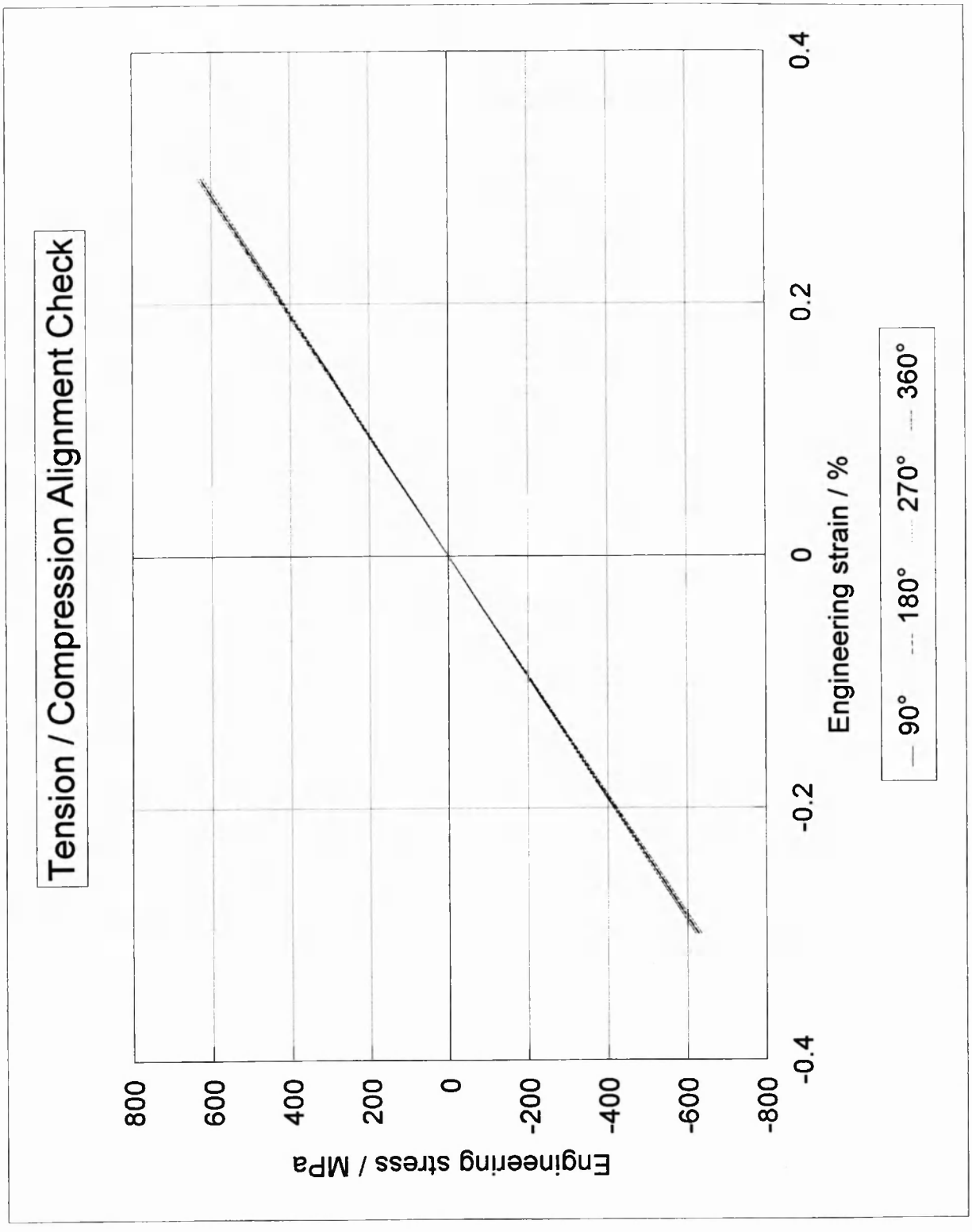

TC test alignment check.

Figure 20

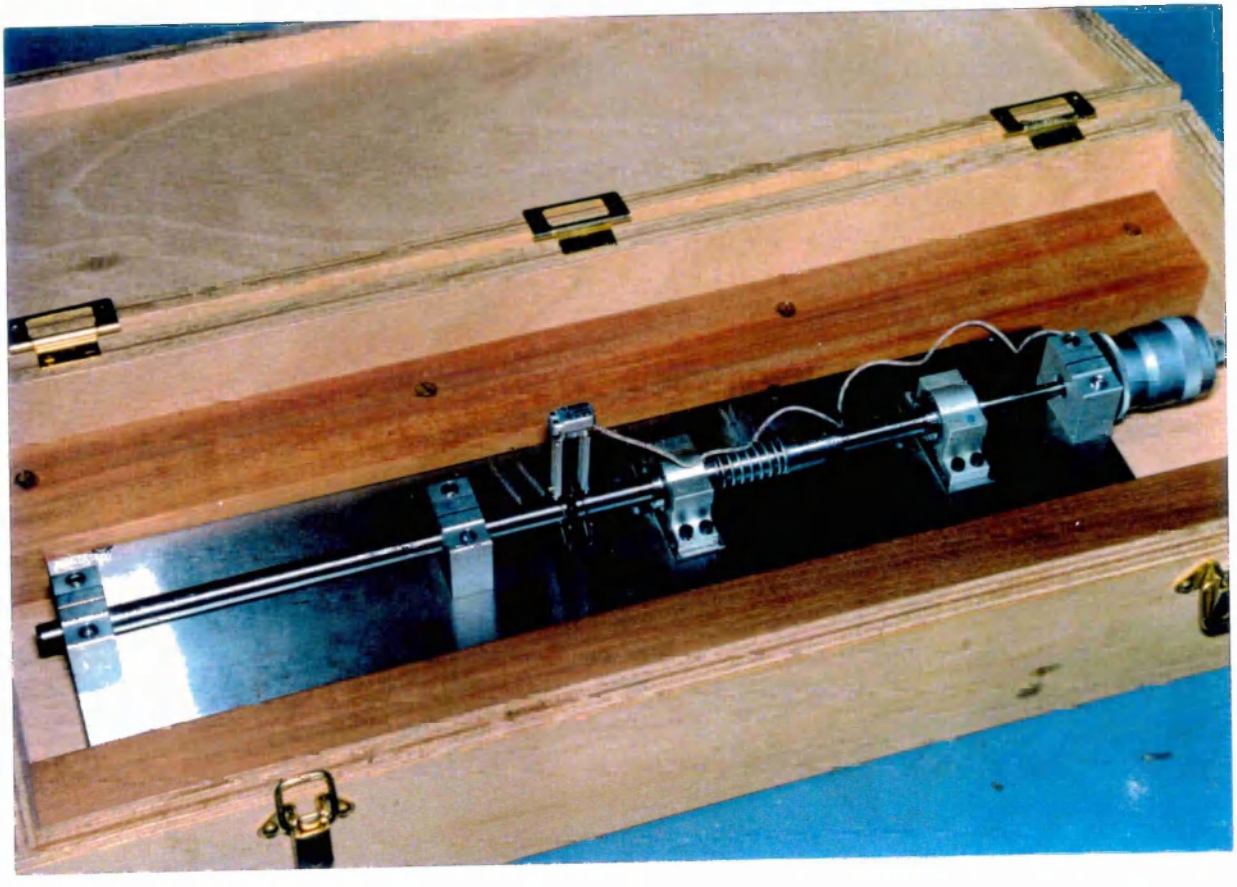

SANDNER 10 - 5X extensometer calibration device.

Figure 21

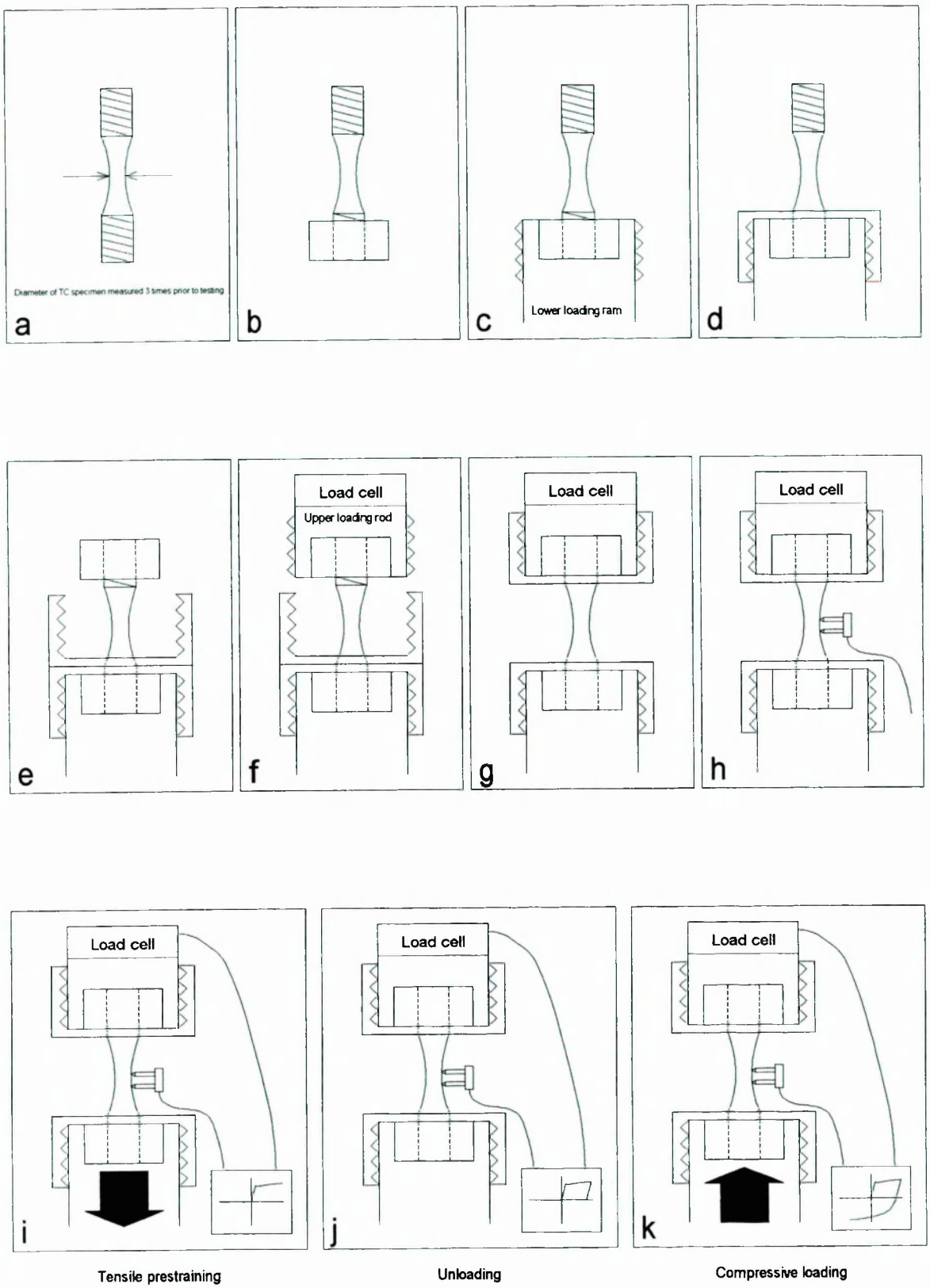

A schematic representation of the installation and testing of a TC test specimen.

Figure 22

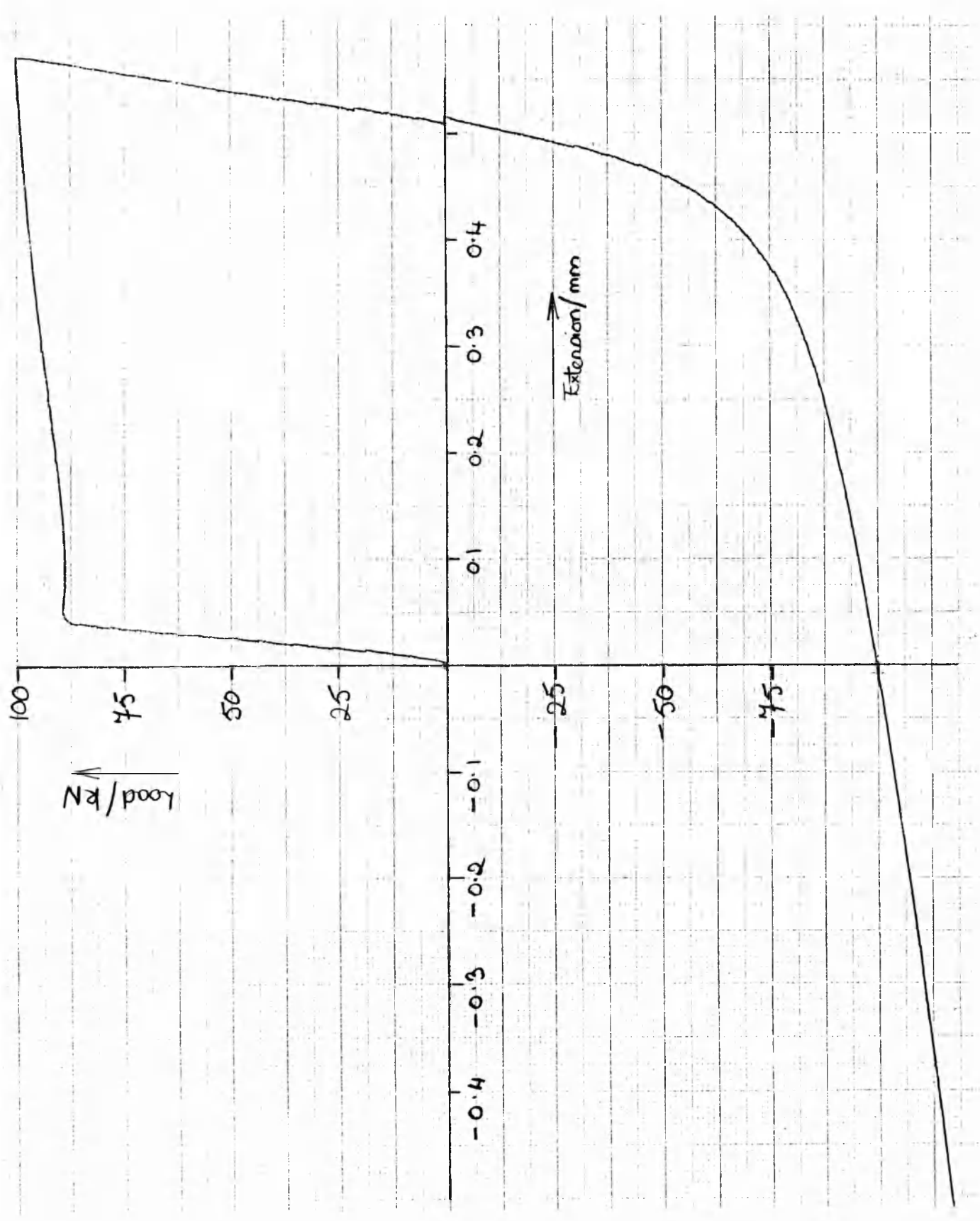

Load / extension curve associated with the testing of a TC specimen given a tensile prestrain of 5.1%.

Figure 23

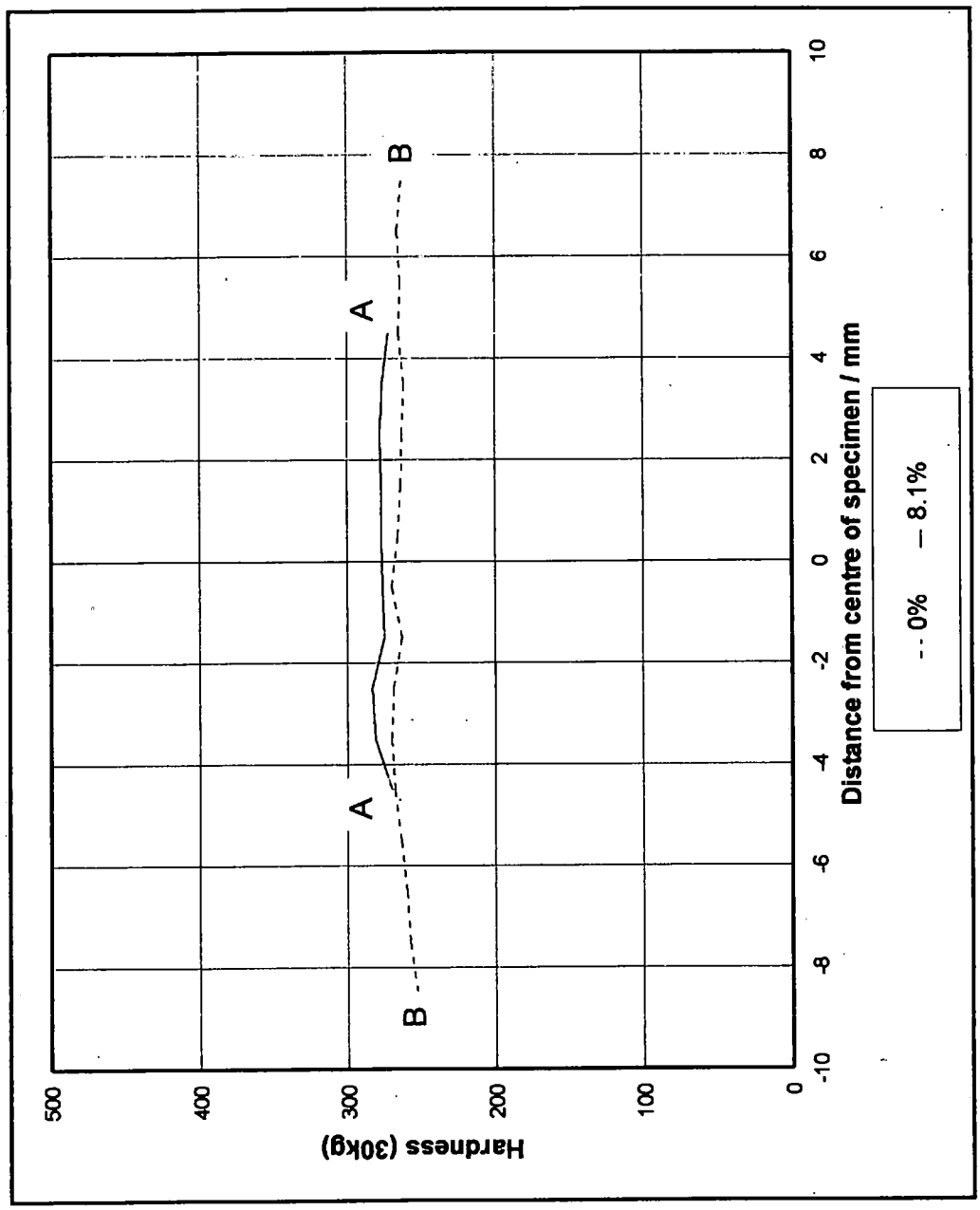

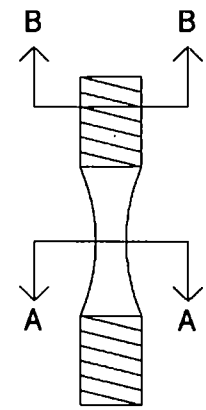

Hardness profile across a TC specimen before and after a tensile prestrain of 8.1%.

Figure 24

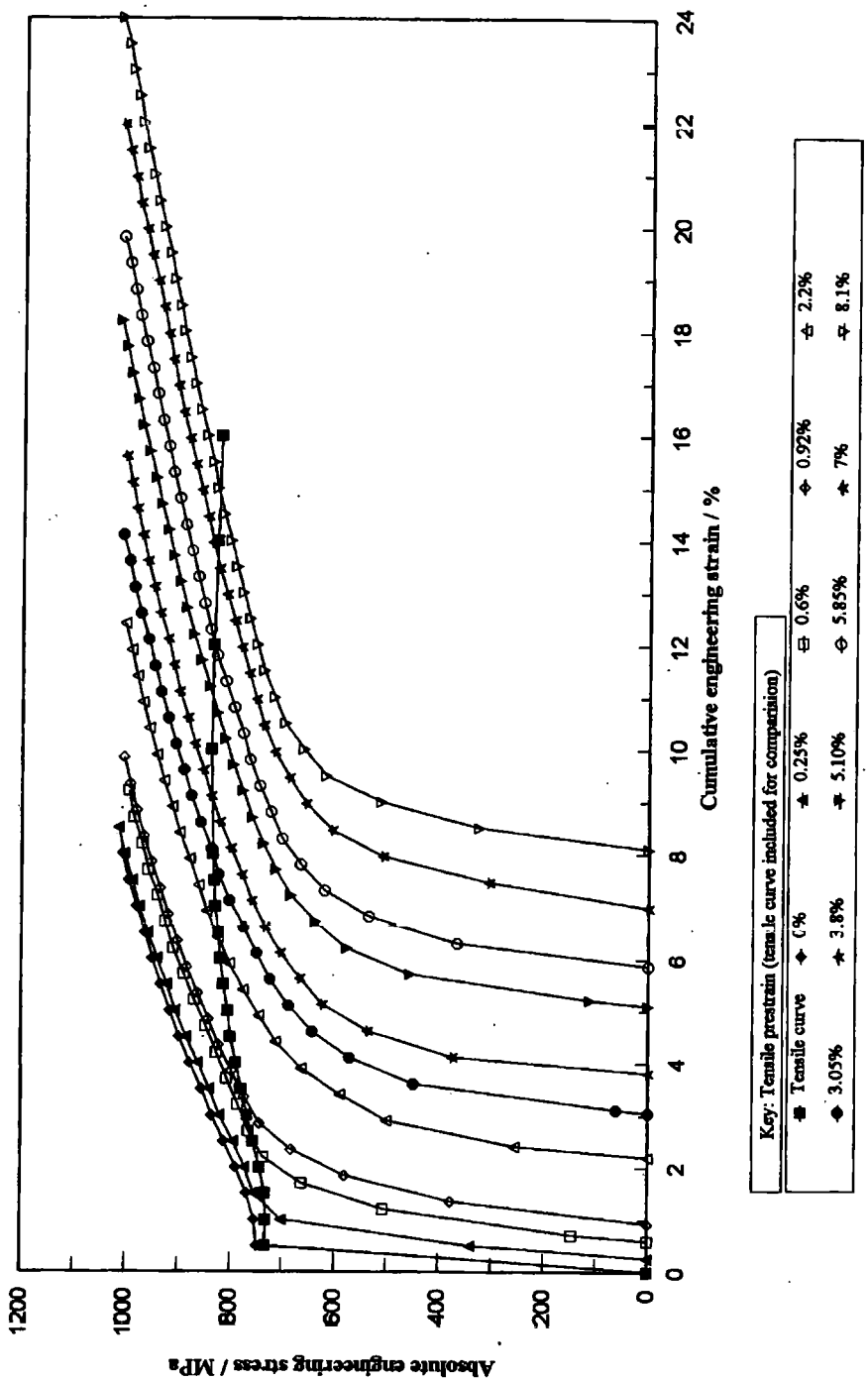

Reverse σ / ϵ curves for Q2N after various amounts of tensile engineering prestrain, ranging from 0% to 8.1% plotted in terms of absolute engineering stress and cumulative engineering strain.

Figure 25

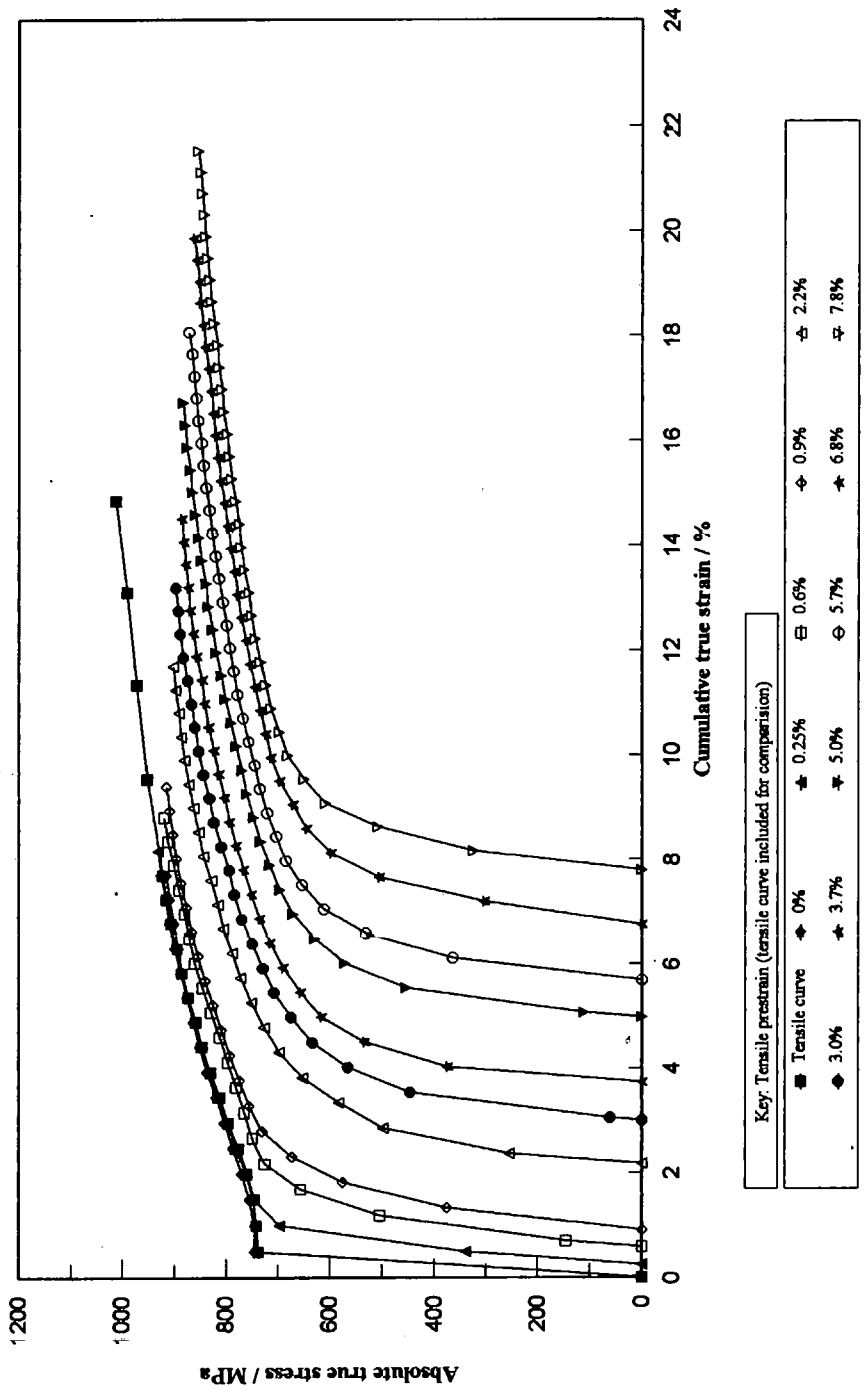

Reverse σ / ϵ curves for Q2N after various amounts of tensile true prestrain, ranging from 0% to 7.8% plotted in terms of absolute true stress and cumulative true strain.

Figure 26

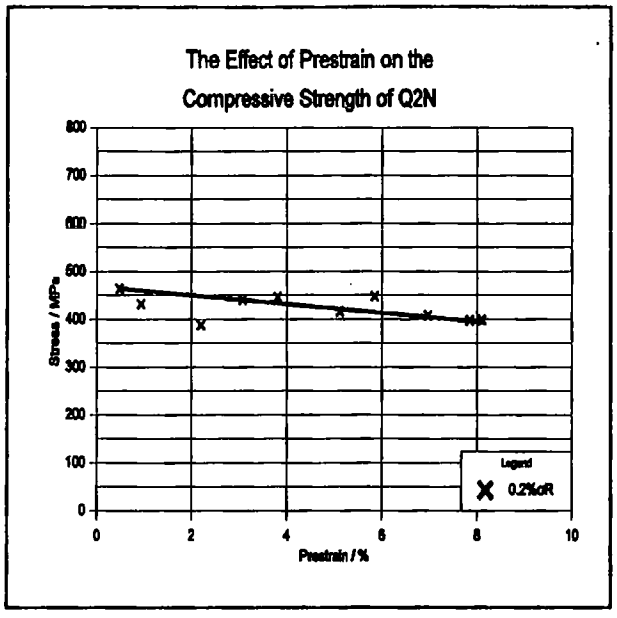

(a) The effect of tensile prestrain on the 0.2% compressive proof stress of Q2N.

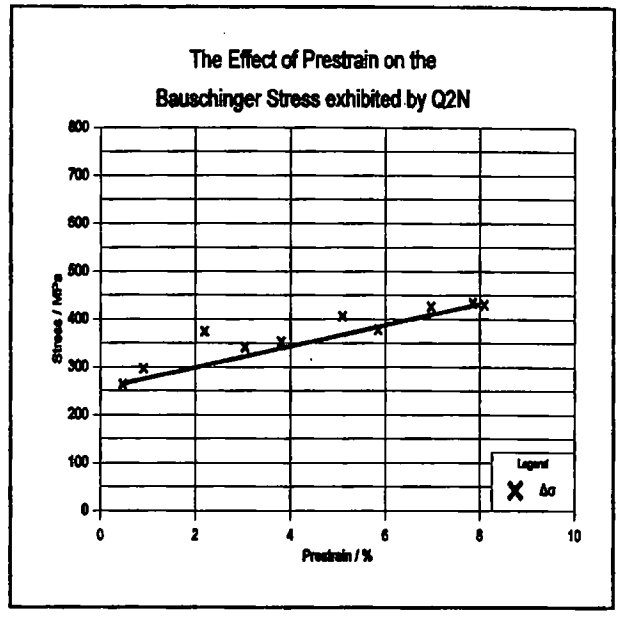

(b) The effect of tensile prestrain on the Bauschinger stress exhibited by Q2N.

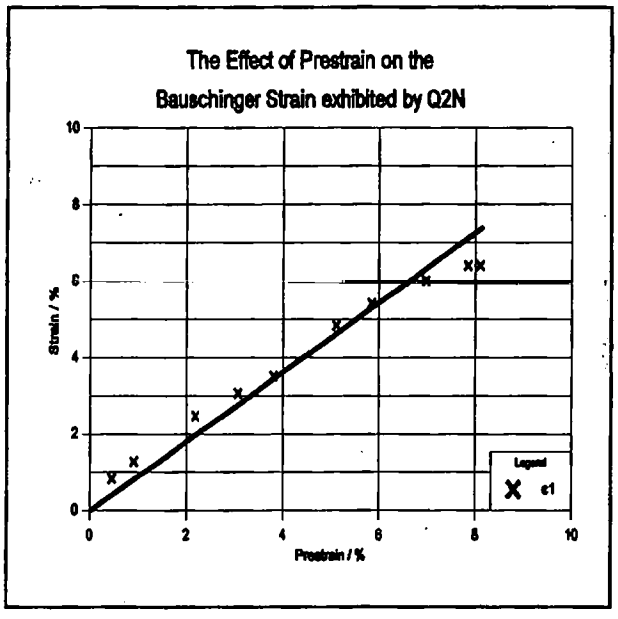

(c) The effect of tensile prestrain on the Bauschinger strain exhibited by Q2N.

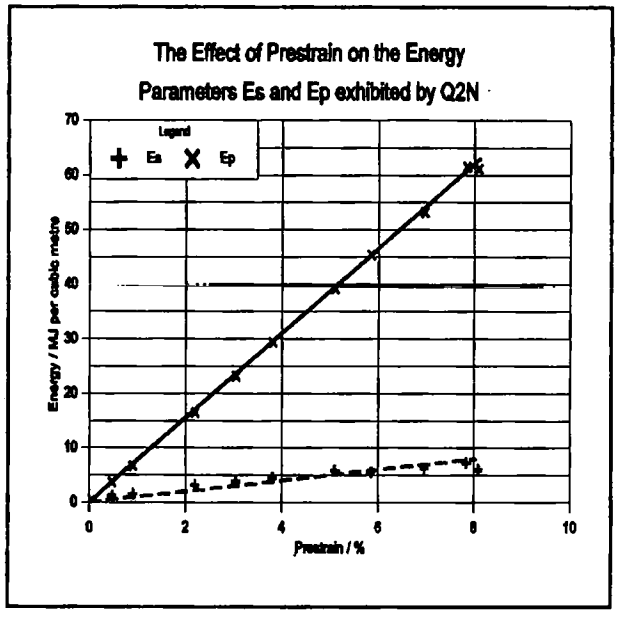

(d) The effect of tensile prestrain on the Bauschinger energy parameters E_S and E_P exhibited by Q2N.

Figure 27

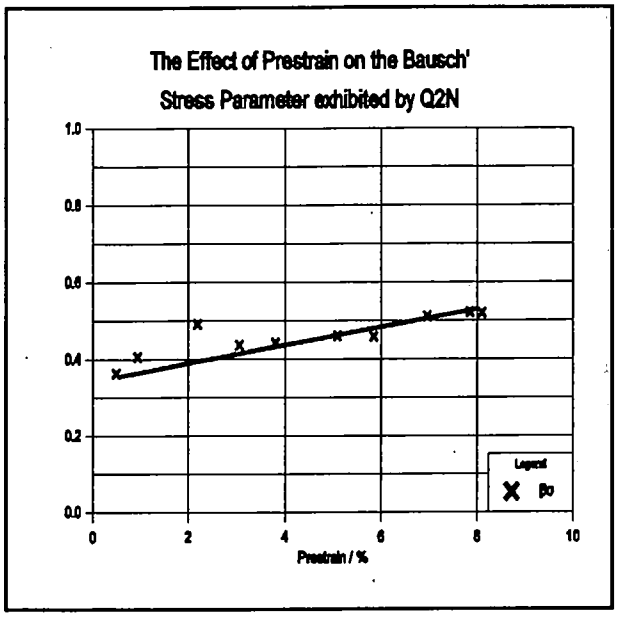

(e) The effect of tensile prestrain on the Bauschinger stress parameter exhibited by Q2N.

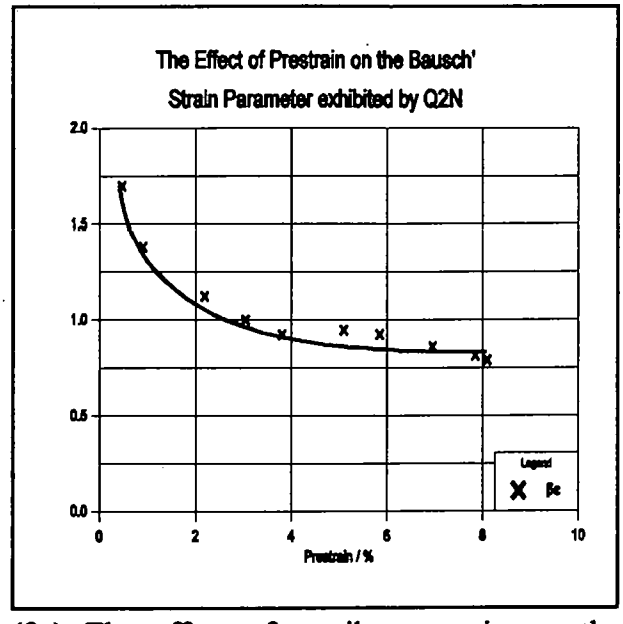

(f) The effect of tensile prestrain on the Bauschinger strain parameter exhibited by Q2N.

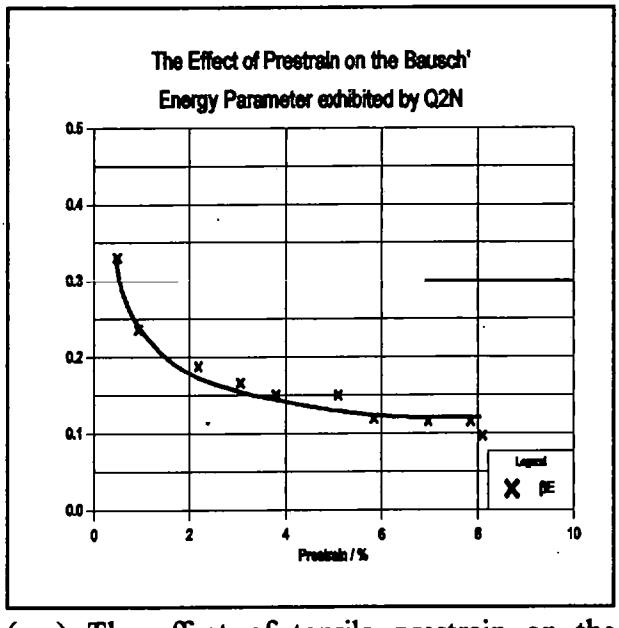

(g) The effect of tensile prestrain on the Bauschinger energy parameter exhibited by Q2N.

Figure 27 continued

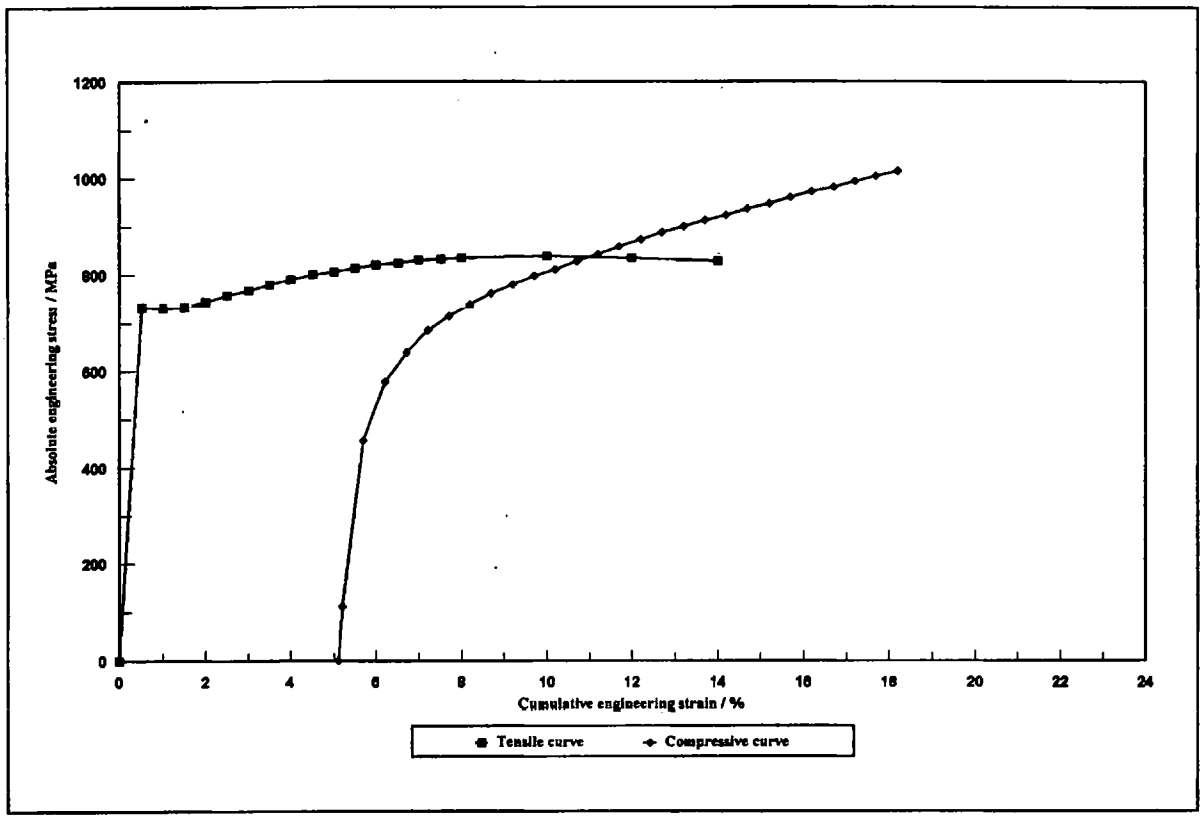

(a) Compressive σ / ϵ for Q2N after a tensile engineering prestrain of 5.1% plotted in terms of absolute engineering stress and cumulative engineering strain.

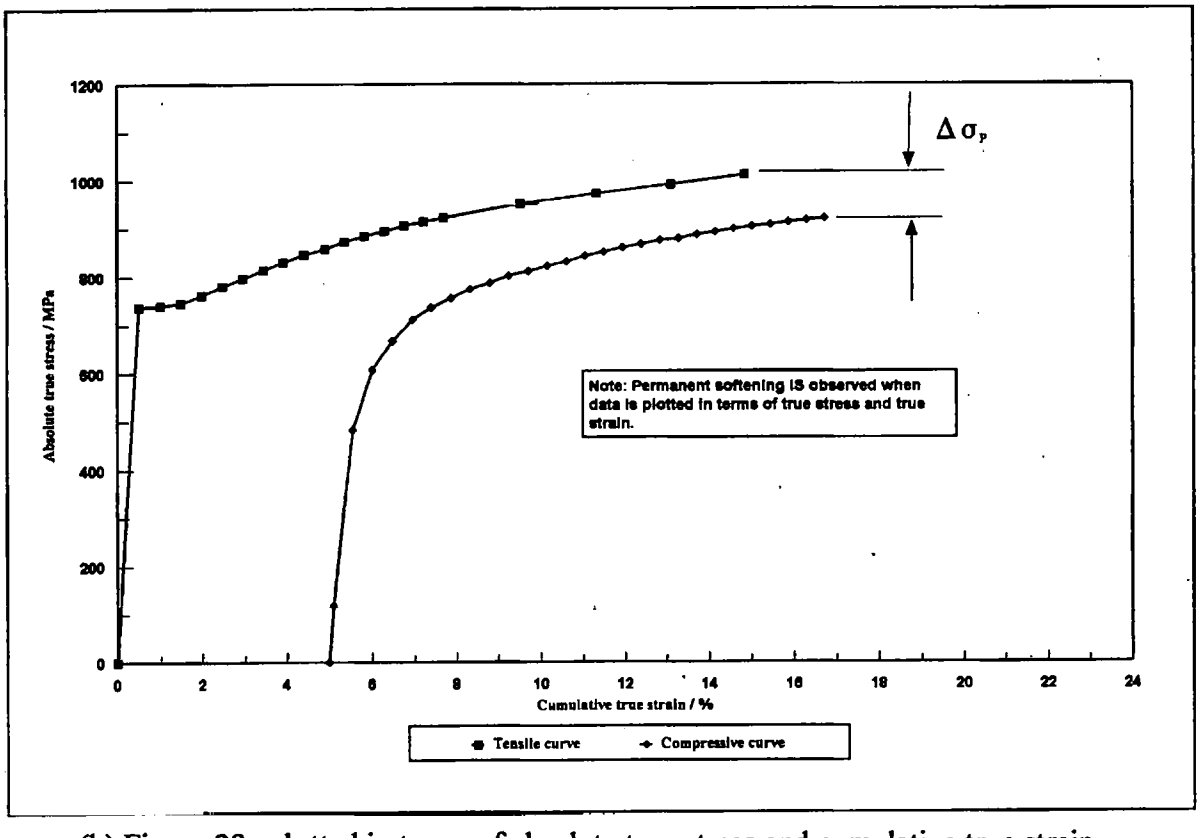

(b) Figure 28a plotted in terms of absolute true stress and cumulative true strain.

Figure 28

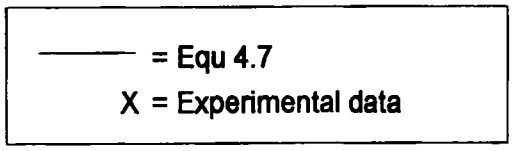

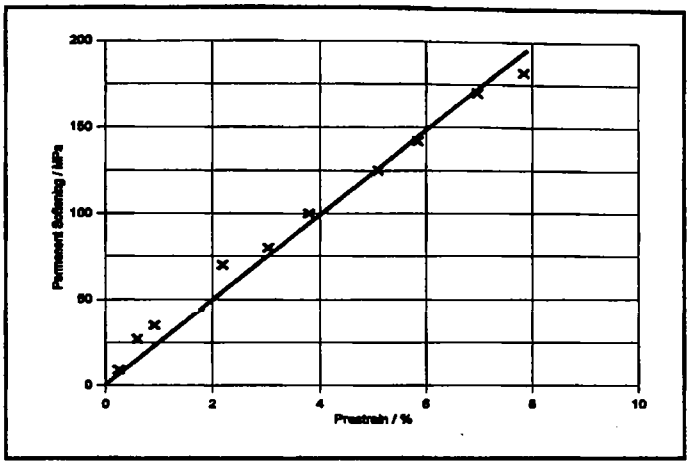

(a)Experimental values of permanent softening, $\Delta\sigma_p$, exhibited by Q2N.

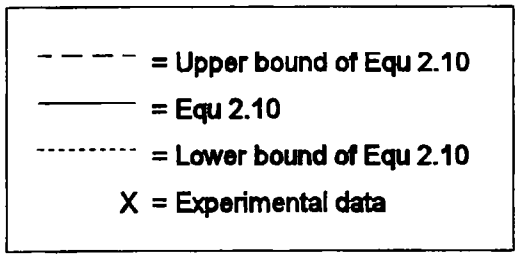

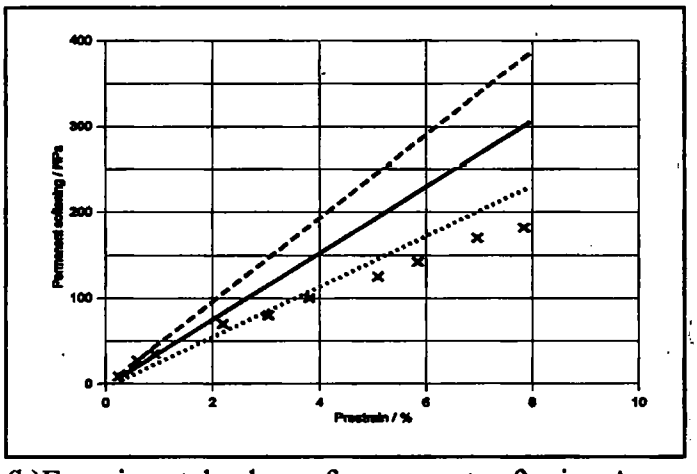

(b)Experimental values of permanent softening, $\Delta\sigma_p$, exhibited by Q2N presented in conjunction with Equation 2.10 and its upper and lower bounds.

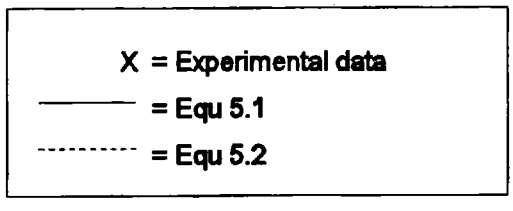

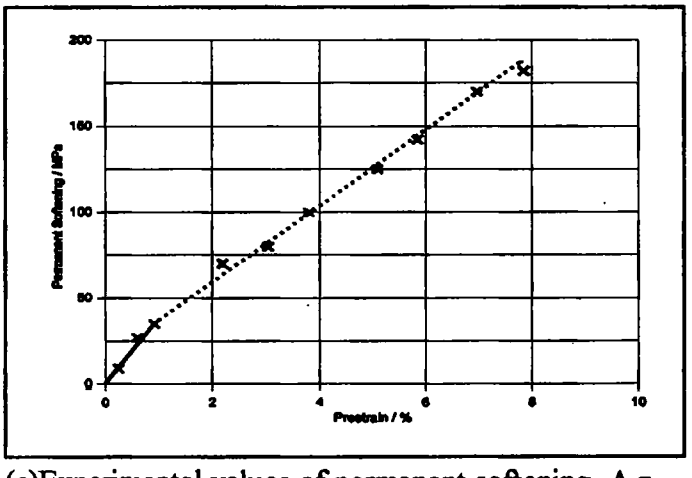

(c)Experimental values of permanent softening , $\Delta\sigma_p$, exhibited by Q2N fitted with a compound curve associated with matrix / particle interfacial breakdown / decohesion.

Figure 29

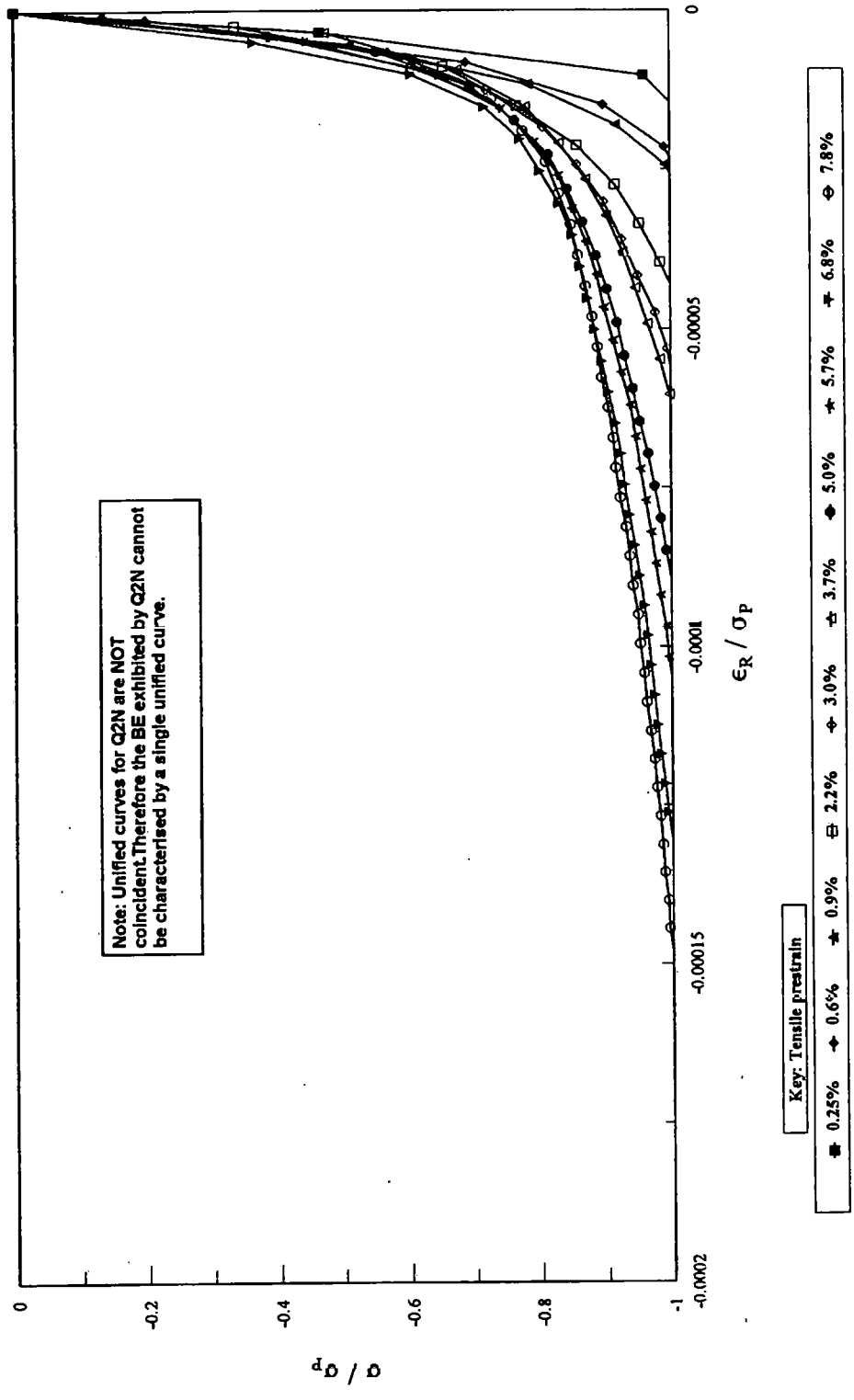

Unified curves for Q2N derived from true σ / ϵ curves (Fig. 26) for prestrains ranging from 0.25% to 7.8%.

Figure 30

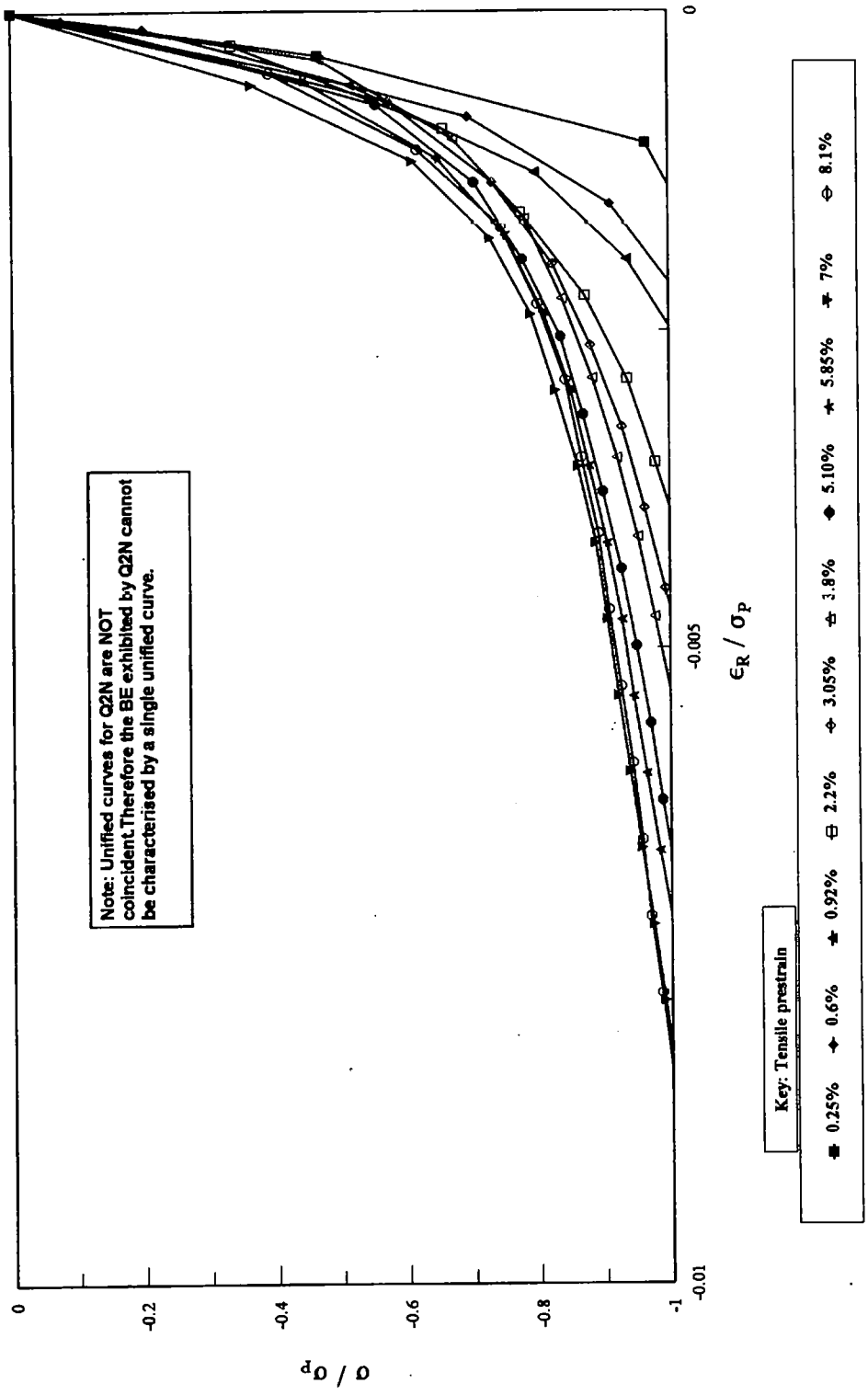

Unified curves for Q2N derived from engineering σ / ϵ curves (Fig. 25) for prestrains ranging from 0.25% to 8.1%.

Figure 31

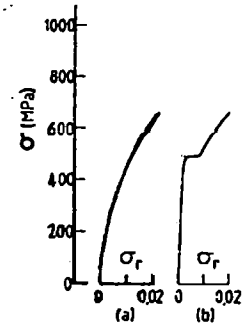

(a) Reverse curve for specimen tested in compression immediately after being prestrained in tension.

(b) Reverse curve for specimen heat treated at 200°C for 30 mins prior to being tested in compression.

The effect of heat treatment on the Bauschinger effect exhibited by mild steel [25].

Figure 32

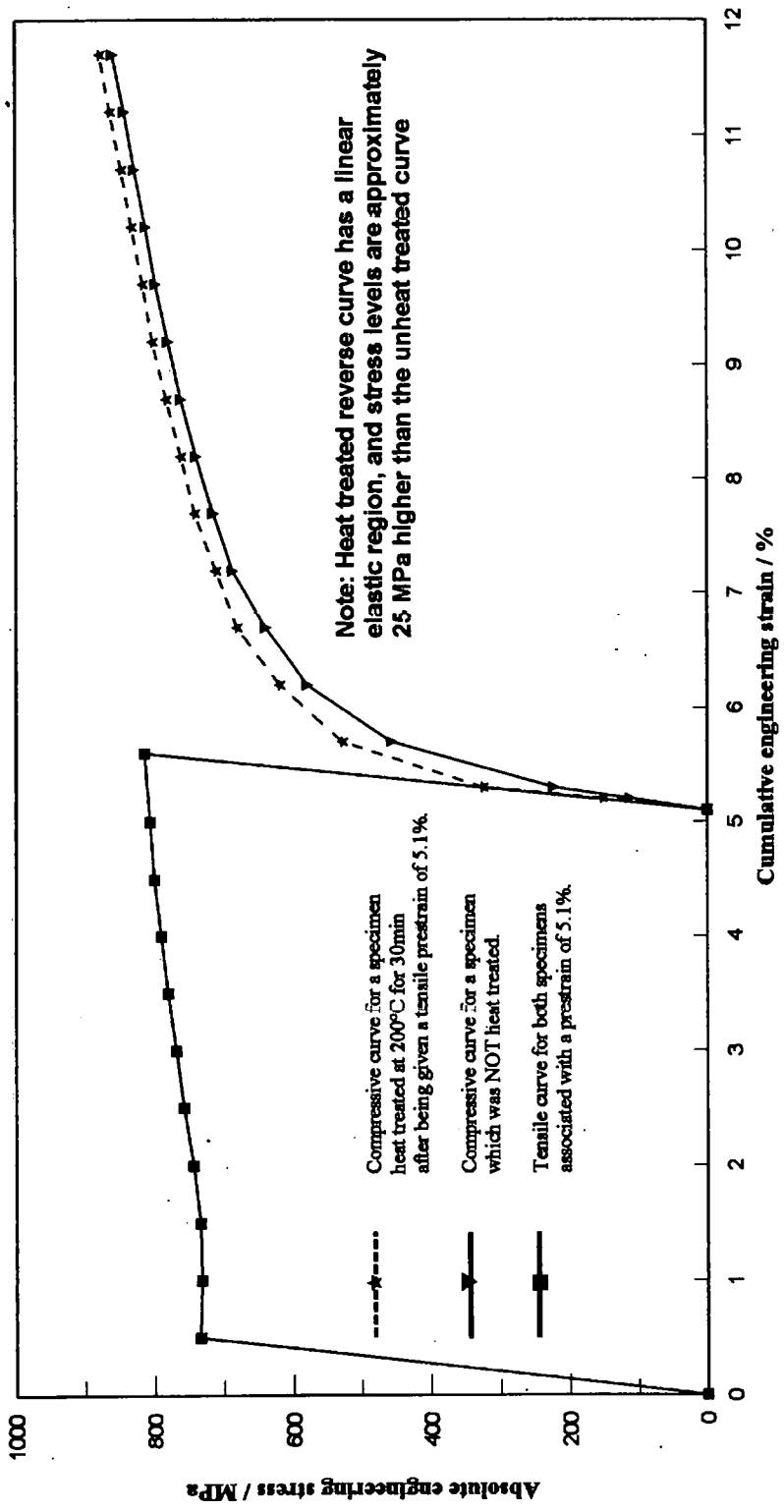

The effect of heat treatment on the BE exhibited by Q2N.

Figure 33

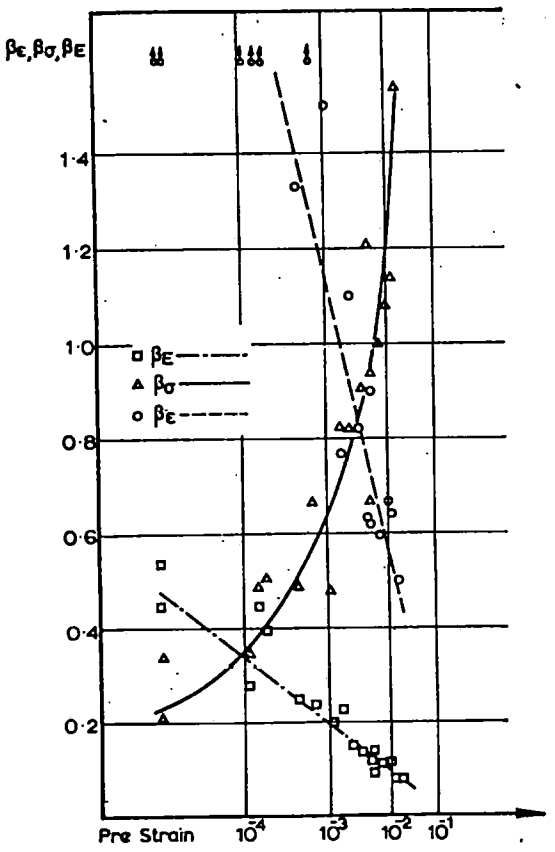

The effect of prestrain on secondary BE parameters [24]

Figure 34

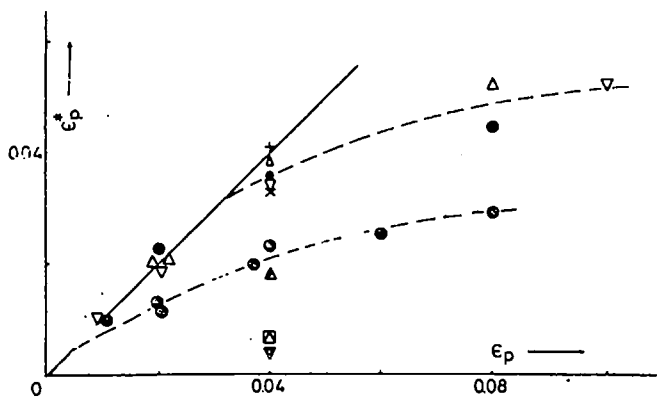

Note: Although ϵ_p^* is not a direct measure of permanent softening, $\Delta\sigma_p$, it is proportional to $\Delta\sigma_p$.

The effect of tensile prestrain on the permanent softening (ϵ_p^*) exhibited by Cu - SiO_2 [2]

Figure 35

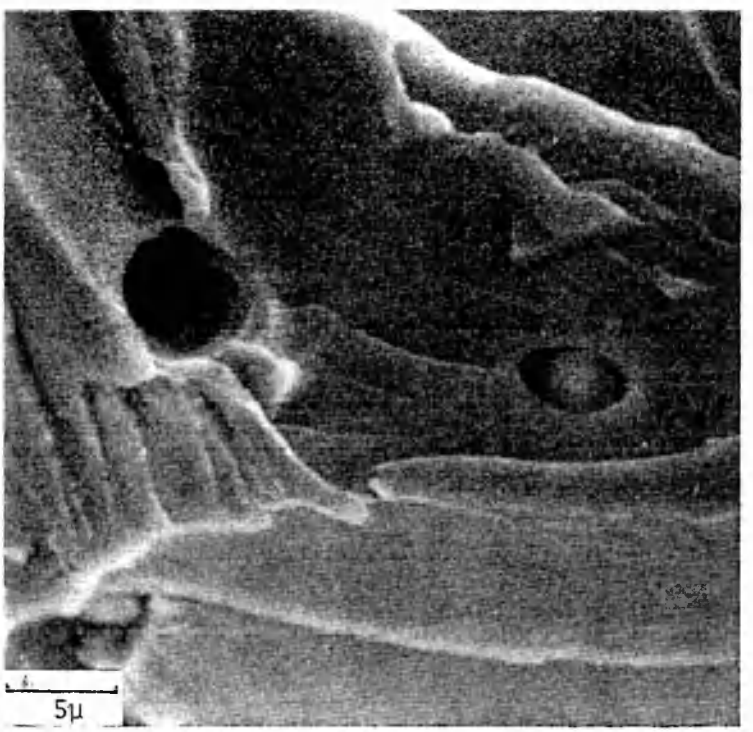

Scanning electron micrograph of cleaved iron showing a silica inclusion within an elongated void, indicative of plastic matrix / elastic particle interfacial breakdown. [31]

Figure 36